Mean evaporation and condensation coefficients based on energy dependent condensation probability

Maurice Bond and Henning Struchtrup*
Department of Mechanical Engineering, University of Victoria, P.O. Box STN CSC 3055, Victoria, British Columbia, Canada V8W 3P6
(Received 3 September 2004; published 22 December 2004)

A generalization of the classical Hertz-Knudsen and Schrage laws for the evaporation mass and energy fluxes at a liquid-vapor interface is derived from kinetic theory and a simple model for a velocity dependent condensation coefficient. These expressions, as well as the classical laws and simple phenomenological expressions, are then considered for the simulation of recent experiments [G. Fang and C. A. Ward, Phys. Rev. E **59**, 419 (1999)]. It is shown that mean condensation and evaporation coefficients in the mass flow influence the results only if they are small compared to unity and that the expression for evaporation mass flow determines the temperature of the liquid. Moreover, it is shown that the expression for evaporation energy flow plays the leading role in determining the interface temperature jump, which can be obtained in good agreement with the experiment from the generalized kinetic theory model and phenomenological approaches, but not from the classical kinetic-theory-based Hertz-Knudsen and Schrage laws. Analytical estimates show that the interface temperature jump depends strongly on the temperature gradient of the vapor just in front of the interface, which explains why much larger temperature jumps are observed in spherical geometry and the experiments as compared to planar settings.

DOI: 10.1103/PhysRevE.70.061605 PACS number(s): 68.03.Fg, 64.70.Fx, 51.10.+y, 47.45.Nd

I. INTRODUCTION

While evaporation and condensation phenomena have been a subject of research and debate for more than 100 years, the mechanism of transfer across a phase boundary was not a great focus of research because it was considered adequate to assume that the liquid-vapor interface is nearly at complete equilibrium. In particular this led to the assumption that at the interface both phases have the same temperature, even outside of equilibrium. See Ref. [1] for a good overview of the history of this topic.

Just recently, a series of steady-state evaporation and condensation experiments performed at the University of Toronto by Ward, Fang, and Stanga [2–4] exhibited large positive temperature jumps of up to $T_v - T_l \simeq 7.8\ ^\circ\mathrm{C}$ across the interface, something not previously observed. These experiments, in the following referred to as "Toronto experiments," triggered new interest in the field, including the results presented here.

The main quantity of interest in evaporation and condensation problems is the evaporation rate j, which is defined as positive in the case of evaporation and is negative in the case of condensation. In many theories its computation involves mean evaporation and condensation coefficients, which are, loosely speaking, the probabilities for a liquid particle to evaporate and for a vapor particle to condense. There are two main roads to compute j (or the coefficients): either by means of kinetic-theory-based arguments or by using ideas of thermodynamics of irreversible processes (TIP).

Our subsequent analysis will show that knowledge of j is not sufficient to successfully simulate, and understand, evaporation and condensation, but that an expression for the evaporation energy flux Q is indispensable. Also Q is determined through mean evaporation and condensation coefficients, which may, but must not necessarily, have the same values as the mean coefficients appearing in j.

Expressions for j and Q are derived in kinetic theory by means of approximate solutions of the Boltzmann equation, in particular those obtained by the Chapman-Enskog method, and require microscopic condensation probabilities as an input to compute mean values. In most of the literature, the microscopic condensation probability is assumed to be constant [5–11], but molecular dynamic (MD) simulations show that it indeed depends on the impact energy of a vapor particle that hits the liquid as well as on the temperature T_l of the liquid surface. See Ref. [12] for an overview on molecular dynamic approaches and [13–16] for more detailed molecular dynamic simulations.

In Refs. [16,17] the authors propose a condensation coefficient of the form

$$\theta_c = \psi\left[1 - \omega\exp\left(\frac{-E_{mol}}{RT_l}\right)\right], \tag{1}$$

where E_{mol} is the translational molecular energy in the direction normal to the surface, R is the gas constant, and ψ and ω are constants that describe the details of the condensation probability. In Ref. [16] it is also observed that most vapor molecules that do not condense exchange energy with the liquid and are thermalized.

The energy dependent coefficient (1) was used in direct simulation Monte Carlo (DSMC) simulations [18], but to our knowledge it has not been used so far to compute expressions for the mass and energy fluxes through the interface, j and Q. This task will form the first part of this paper, where

*Electronic address: struchtr@me.uvic.ca

we use expression (1) together with approximate velocity distribution functions at the interface to compute and discuss expressions for j and Q. Our expressions turn out to be more general than expressions normally obtained from kinetic theory, but reduce to classical models—e.g., the classical Hertz-Knudsen expressions [5,6] or the Schrage correction [1] to these—for certain choices of the parameters.

As we proceed, it will be seen that the values of the coefficients ψ and ω have a marked influence on the temperature jump at the interface. In particular they can be chosen such that the temperature jump is positive, while the classical models, which assume a constant coefficient (i.e., $\omega=0$), will in most cases lead to small negative jumps.

After discussing kinetic-theory-based expressions for Q and j we briefly discuss simple models based on TIP [19–22]. These models find expressions for j and Q by assuming linear laws between "thermodynamic fluxes" and "thermodynamic forces" that guarantee positive entropy generation at the interface.

Ward and Fang [23,24] suggested statistical rate theory (SRT) as an alternative to kinetic theory and TIP, and we shall discuss their expression for j in relation to TIP. Unfortunately, SRT does not provide an expression for the energy flux Q, and in order to complete the SRT model, we decided to employ the TIP expression for Q.

A popular configuration for studying one-dimensional evaporation and condensation phenomena is the parallel surface geometry [7,8,21,25–28], a topic that goes beyond the scope of this paper and will not be further discussed. Another interesting recent approach to the topic is the Van der Waals square gradient model [29–31], which also shall not be discussed further.

After discussing the theory behind the expressions for j and Q, we next consider simple one-dimensional models in planar, spherical, and mixed planar and spherical geometries, which approximate the conditions of the Toronto experiments [2–4] where only the boundary temperatures of liquid and vapor and the pressure in the vapor were prescribed. The balances of mass and energy are solved for the liquid and vapor temperature profiles. The complete solution requires the expressions for mass and energy flux across the interface, developed from kinetic theory, SRT, and TIP. The analysis is performed for relatively slow evaporation and condensation. The equations are solved to yield the mass and energy fluxes per unit area and the liquid and vapor temperature profiles.

Before presenting some numerical solutions, we do a simple analysis of the results based on the order of magnitude of certain terms in the solutions and equations. The findings are then supported by the numerical solutions. In particular we shall show that, at least for the conditions of the Toronto experiment, the following holds.

(i) The condensation and evaporation coefficients in the mass flow j influence the results only if they are very small compared to unity.

(ii) The expression for mass flow j determines the temperature of the liquid, which is close to the saturation temperature $T_{sat}(p_v)$ where p_v is the pressure prescribed in the vapor.

(iii) The expression for energy flow Q plays the leading role in determining the interface temperature jump, which can be obtained in good agreement to the experiment by adjusting the parameters ψ, ω in Eq. (1) or the phenomenological coefficients in the TIP-based models.

(iv) The interface temperature jump depends strongly on the temperature gradient of the vapor at the interface.

(v) The last finding explains why much larger temperature jumps are observed in spherical geometry, as compared to planar settings.

(vi) And, finally, the Toronto experiment is better described by a mixed planar-spherical geometry, which might explain the large temperature jump observed.

The remainder of the paper is organized as follows.

Section II recalls some basic results from kinetic theory, and Sec. III discusses the vapor distribution function at the interface and introduces evaporation and condensation coefficients. This forms the base of the derivations of the generalized Hertz-Knudsen and Schrage laws for evaporation mass and energy fluxes in Secs. IV and V. Phenomenological theories for evaporation mass and energy fluxes, including those based on statistical rate theory, are briefly presented in Sec. VI. Section VII discusses the experimental setup and the solution of the governing equations for simple geometries that mimic the experiment. The analytical solutions are then considered in Sec. VIII in an approximative manner to estimate the importance of various terms in the equations. The findings there are then supported by numerical solutions in Sec. IX. Finally we briefly review our findings and present the conclusions.

II. VELOCITY DISTRIBUTION FUNCTION AND MOMENTS

In kinetic theory, the behavior of a system of molecules is described by the distribution function $f(c_i,x_i,t)$, which is defined such that $f(c_i,x_i,t)d\mathbf{c}d\mathbf{x}$ is the number of molecules with velocities in $\{\mathbf{c},\mathbf{c}+d\mathbf{c}\}$ and positions in $\{\mathbf{x},\mathbf{x}+d\mathbf{x}\}$, at time t. Knowledge of the distribution function allows the computation of bulk properties such as mass density

$$\rho = m\int_{-\infty}^{\infty} f d\mathbf{c}, \tag{2}$$

momentum density

$$\rho v_i = \int_{-\infty}^{\infty} mc_i\, f d\mathbf{c}, \tag{3}$$

internal energy

$$\rho u = \frac{3}{2}p = \frac{3}{2}\rho RT = \int_{-\infty}^{\infty} \frac{m}{2}C^2 f d\mathbf{c}, \tag{4}$$

pressure tensor

$$p_{ij} = \int_{-\infty}^{\infty} mC_iC_j\, f d\mathbf{c}, \tag{5}$$

and heat flux

$$q_i = \int_{-\infty}^{\infty} \frac{m}{2} C^2 C_i \, f d\mathbf{c}. \tag{6}$$

Here, m denotes the molecular mass, $R=k/m$ is the gas constant where k denotes Boltzmann's constant, $C_i=c_i-v_i$ is the peculiar velocity, v_i is the mean velocity, and p denotes the pressure which is related to temperature and density by the ideal gas law $p=\rho RT$.

In the following, we shall be mostly interested in the fluxes of mass and energy through a vapor-liquid interface (in normal direction). When the normal of the interface points into the $x_3=z$ direction, these are defined as

$$j = \int_{-\infty}^{\infty} m c_z \, f d\mathbf{c} \tag{7}$$

and

$$Q = \int_{-\infty}^{\infty} \frac{m}{2} c_z c^2 f d\mathbf{c}, \tag{8}$$

respectively.

The velocity distribution f is determined by the Boltzmann equation [32]

$$\frac{\partial f}{\partial t} + c_i \frac{\partial f}{\partial x_i} = \mathcal{S}(f), \tag{9}$$

where $\mathcal{S}(f)$ denotes the collision term, which describes the change of the velocity distribution due to intermolecular collisions. The balance laws for mass, momentum, and energy, as well as the H theorem, can be derived by suitable averaging of the Boltzmann equation over the microscopic velocity [32,33].

In equilibrium, the velocity distribution function does not change with time or location and the collision term must vanish, which implies that the equilibrium distribution is the Maxwellian [32]

$$f_M(p,T,C) = \frac{p}{mRT} \frac{1}{\sqrt{2\pi RT}^3} \exp\left(-\frac{C^2}{2RT}\right). \tag{10}$$

Nonequilibrium solutions of the Boltzmann equation are considerably more complex. The Boltzmann equation can be solved by computer either directly or by DSMC simulations [34], both of which are computationally expensive.

The Chapman-Enskog (CE) method expands the distribution function about the Knudsen number N_{Kn}. The Knudsen number is the ratio of the mean distance a molecule travels between collisions (mean free path) to a macroscopic length associated with the vapor. The first-order CE expansion of the Boltzmann equation gives the distribution function as [35]

$$f_{CE} = f_M\left(1 - \frac{2}{5}\frac{\kappa}{Rp} C_k \left(\frac{C^2}{2RT^2} - \frac{5}{2T}\right)\frac{\partial T}{\partial x_k} + \frac{1}{5}\frac{\kappa}{Rp}\frac{C_k C_i}{RT} \times \left(\frac{\partial v_i}{\partial x_k} + \frac{\partial v_k}{\partial x_i} - \frac{2}{3}\frac{\partial v_r}{\partial x_r}\delta_{ik}\right)\right), \tag{11}$$

where κ is the thermal conductivity. In particular this distribution gives the laws of Fourier,

$$q_i = -\kappa \frac{\partial T}{\partial x_i}, \tag{12}$$

and Navier and Stokes,

$$p_{ik} = p\,\delta_{ik} + \mu\left(\frac{\partial v_i}{\partial x_k} + \frac{\partial v_k}{\partial x_i} - \frac{2}{3}\frac{\partial v_r}{\partial x_r}\delta_{ik}\right), \tag{13}$$

where $\mu=\frac{4}{15}\kappa/R$ is the viscosity. In this paper we shall ignore shear stresses, so that $p_{ik}=p\,\delta_{ik}$; then, the CE distribution reduces to

$$f_{CE} = f_M\left(1 - \frac{2}{5}\frac{\kappa}{Rp} C_k \left(\frac{C^2}{2RT^2} - \frac{5}{2T}\right)\frac{\partial T}{\partial x_k}\right). \tag{14}$$

For equilibrium conditions, in particular vanishing temperature gradient $\partial T/\partial x_k=0$, the CE distribution reduces to the Maxwellian.

III. DISTRIBUTION FUNCTION AT THE INTERFACE

When a particle in the vapor phase hits the liquid-vapor interface, it will undergo an interaction with the liquid particles at the interface. Depending on the microscopic conditions for the particular interaction, the particle can be absorbed by the liquid—i.e., it condenses—or it might be reflected back into the vapor.

The energy of liquid particles at the interface fluctuates due to stochastic interactions between particles. Occasionally a particle gains enough energy to leave into the vapor—the particle is evaporated.

Obviously, evaporation and condensation processes will influence the distribution function at the interface and determine the rates of mass and energy transfer over the interface in nonequilibrium situations.

In a somewhat simplified model, condensation and evaporation processes can be described by several coefficients, which we shall discuss now.

A. Condensation coefficient

The condensation coefficient θ_c is defined as the ratio of incident molecules sorbed by the surface to those which actually hit the surface. Molecules which do not condense are reflected back into the vapor. Accordingly, $\theta_c=1$ if all incident molecules condense and $\theta_c=0$ if all molecules are reflected. Early theories of condensation, in particular the classical Hertz-Knudsen theory [5,6], assume a condensation coefficient $\theta_c=1$, and that assumption is still used regularly; e.g., see Ref. [11].

Molecular dynamic simulations suggest that the condensation coefficient depends on the energy of the incident molecules and the interface surface temperature [14–18]. An incident molecule with high energy can penetrate more deeply into the liquid phase, where it will undergo many interactions with liquid molecules; this increases its likelihood of condensation, since the condensing particle will dissipate energy to the liquid [16]. A higher surface temperature increases the energy of the surface molecules and thus the likelihood of incident molecules having collisions directly at the surface. This reduces incident molecule penetration, which results in

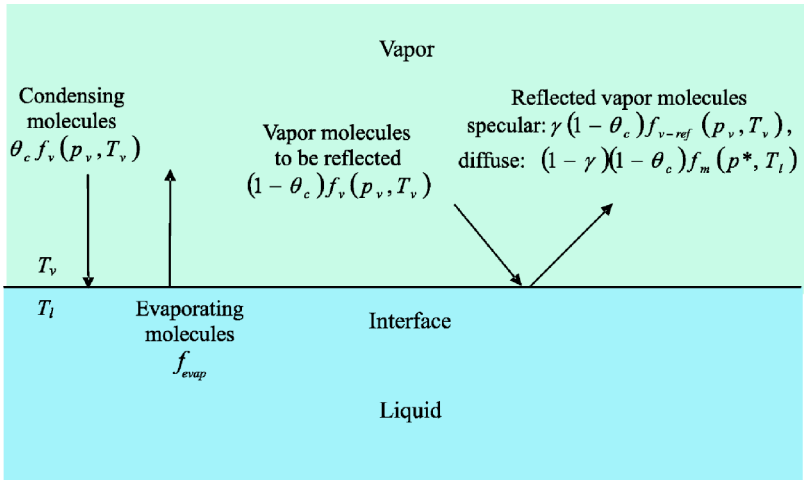

FIG. 1. Velocity distributions at the interface.

a smaller condensation coefficient. To accommodate this behavior, Tsuruta *et al.* suggested that the condensation coefficient is of the form [16]

$$\theta_c = \psi\left[1 - \omega \exp\left(\frac{-c_z^2}{2RT_l}\right)\right], \tag{15}$$

where ψ and ω are constants, T_l is the temperature of the liquid at the interface, and c_z is the particle velocity with respect to the interface, normal to the interface. We shall use this expression below to compute average condensation coefficients. Note that for $\omega=0$ the condensation coefficient is a constant.

Due to its definition, the condensation coefficient must lie between 0 and 1; this must also be true for Eq. (15). If $c_z^2 \to \infty$, $\theta_c=\psi$ so that $0\leqslant\psi\leqslant 1$. For $c_z^2=0$, $\theta_c=\psi(1-\omega)$; this requires $\omega\leqslant 1$ and also implies $\omega\geqslant 1-1/\psi$. Moreover, since the condensation probability of a molecule should increase with its energy mc_z^2 and decrease with higher surface temperature T_l, ω should be positive, so that ω is restricted to $0\leqslant\omega\leqslant 1$. Tsuruta *et al.* [16] report from MD simulations for argon that ψ and ω have values of 0.971–0.685 and 0.086–0.554, respectively.

B. Accommodation coefficient

With $\theta_c\neq 1$, there is a portion of particles which hit the liquid interface and then bounce back into the vapor. In general, the rebounding molecules will have exchanged energy and momentum with the liquid particles, and some knowledge about the reflection mechanism is required. We shall adopt the classical Maxwell model, which assumes that molecules interact with the interface in two basic mechanisms: specular and diffuse reflection.

Specular reflection describes molecules that maintain their energy and do not react thermally with the surface. The specularly reflected molecules maintain the distribution of the incident molecules, except with mirrored velocities.

Diffuse reflection describes molecules which do not conserve their energy and undergo a complete thermal interaction with the surface. Diffusely reflected molecules leave in a Maxwellian distribution $f_M(p^*, T_l, C)$ which is determined by the liquid temperature T_l and an effective pressure p^*, which is determined to guarantee the conservation of mass.

To distinguish between specular and diffuse reflection, the accommodation coefficient γ is introduced, with $\gamma=1$ for pure specular reflection and $\gamma=0$ for pure diffuse reflection.

Figure 1 shows the distribution functions of particles traveling towards or away from the interface; the indices l and v denote properties of liquid and vapor, respectively. From the figure it follows that the condition for conservation of particles in reflection that determines p^* read

$$\int_{c_z\geqslant 0} c_z\gamma(1-\theta_c) f_{v\text{-}ref}(p_v,T_v)d\mathbf{c} + \int_{c_z\geqslant 0} c_z(1-\gamma)(1-\theta_c) \times f_M(p^*,T_l)d\mathbf{c} + \int_{c_z\leqslant 0} c_z(1-\theta_c) f_v(p_v,T_v)d\mathbf{c} = 0. \tag{16}$$

C. Evaporation coefficient

The evaporation coefficient θ_e is a measure of how many molecules escape from the surface into the vapor. Several definitions are possible, and here we define the evaporation coefficient such that the distribution of the evaporating molecules is given by $f_{evap}=\theta_e f_M(p_{evap}, T_l, C)$ where p_{evap} is an effective pressure of the evaporating molecules and T_l is the liquid temperature. Note that θ_e is not a constant, but can depend on physical variables of the system, such as T_l, T_v, C, etc. We proceed by discussing the function θ_e as well as the pressure p_{evap}.

From Fig. 1 follows the distribution of particles directly at the interface as

$$f_{c_z>0} = \theta_e f_M(p_{evap},T_l) + \gamma(1-\theta_c) f_{v\text{-}ref}(p_v,T_v) + (1-\gamma)(1-\theta_c) f_M(p^*,T_l),$$

$$f_{c_z<0} = f_v(p_v,T_v). \tag{17}$$

Let us now consider an equilibrium case, where $T_l=T_v=T$ and no net evaporation or condensation occurs, which implies that $C_i=c_i$. In this case, the vapor pressure must be the saturation pressure, $p_v=p_{sat}(T)$, and the distribution (17) must be the Maxwellian at the saturation pressure—i.e.,

$$f_{c_z>0} = \theta_e f_M(p_{evap},T) + \gamma(1-\theta_c) f_M(p_{sat}(T),T) + (1-\gamma)(1-\theta_c) f_M(p^*,T) = f_M(p_{sat}(T),T),$$

$$f_{c_z<0} = f_v(p_v,T_v) = f_M(p_{sat}(T),T). \tag{18}$$

For these particular conditions, Eq. (16) for the pressure p^* reads

$$\int_{c_z\geqslant 0} c_z \gamma(1-\theta_c) \times f_M(p_{sat}(T),T)d\mathbf{c} + \int_{c_z\geqslant 0} c_z(1-\gamma)(1-\theta_c) f_M(p^*,T)d\mathbf{c} + \int_{c_z\leqslant 0} c_z(1-\theta_c) f_M(p_{sat}(T),T)d\mathbf{c} = 0.$$

From Eq. (10) it follows that we can write $f_M(p,T,C) = pF(T,C)$ and thus Eq. (18) can be rewritten as

$$p_{evap}\theta_e + p_{sat}(T)\gamma(1-\theta_c) + p^*(1-\theta_c)(1-\gamma) = p_{sat}(T). \tag{19}$$

Since $\int_{c_z\leqslant 0} c_z(1-\theta_c) f_M(p_{sat}(T),T)d\mathbf{c} = -\int_{c_z\geqslant 0} c_z(1-\theta_c) \times f_M(p_{sat}(T),T)d\mathbf{c}$, the equation for p^* assumes the form

$$(p^* - p_{sat}(T)) \int_{c_z\geqslant 0} c_z(1-\gamma)(1-\theta_c) F d\mathbf{c} = 0.$$

The last equation implies that $p^* = p_{sat}(T)$ in equilibrium, since the integral is different from zero. With this it follows from Eq. (19) that

$$p_{evap}\theta_e = p_{sat}(T)\theta_c$$

must hold in thermal equilibrium. Most notably, this shows that evaporation and condensation coefficients are not independent.

The distribution of evaporating particles in equilibrium (E) is therefore given by

$$f_{evap|E} = \theta_e f_M(p_{evap},T,C) = \theta_e p_{evap} F(T,C) = \theta_c p_{sat}(T) F(T,C) = \theta_c f_M(p_{sat}(T),T,C).$$

This means that in equilibrium the distribution of *evaporating* particles can be expressed by the *condensation* coefficient and the saturation pressure. The same function can be used in nonequilibrium, if one assumes that the nonequilibrium between vapor and liquid has negligible effect on evaporation. Under this assumption, the nonequilibrium evaporation distribution follows from replacing the temperature T by the liquid temperature T_l so that

$$f_{evap} = \theta_c f_M(p_{sat}(T_l),T_l,C). \tag{20}$$

With θ_c given by Eq. (15) it follows that f_{evap} depends *only* on the state of the liquid, through the temperature T_l. Thus, the use of Eq. (20) ignores any effect that the vapor might have on evaporation, such as strong impacts of vapor particles that kick a liquid particle out of the interface. Another assumption inherent in the use of Eq. (20) is that of local equilibrium of the liquid: any gradients in temperature and other quantities in the liquid are assumed to not affect the distribution of evaporating particles.

D. Knudsen layer

In what follows it is assumed that all vapor molecules interacting with the interface have the bulk vapor distribution, while those leaving the interface have a distribution associated with the interface.

In reality, these two different molecular streams interact in a small layer in front of the interface, which alters the distributions of both. The interactions cause the distribution of the escaping molecules to approach that of the bulk vapor. The region where this equilibration occurs is referred to as the Knudsen layer, which typically has a thickness of approximately one mean free path [32].

Within the Knudsen layer, the velocity distributions of both molecule streams can no longer be described by the bulk vapor and interface distributions. The distribution change with location, making it difficult to resolve. Since the incident vapor molecules no longer have the bulk vapor distribution, the characteristics of the vapor near the wall will be altered. However, the effects are usually small, at least for small to intermediate N_{Kn}. Because of this and the complexity of the altered distribution functions, the Knudsen layer is often neglected or set to zero thickness, and incident molecules are assumed to possess the bulk vapor distribution up to the wall. This will be done here as well.

Sone [11], Cercignani [32], Rebrov [36], and Meland and Ytrehus [37] provide a more detailed analysis of the Knudsen layer.

IV. GENERALIZED HERTZ-KNUDSEN THEORY

A. Distribution function

In the previous section we discussed the distribution function at the interface, and now we shall use the results to compute the evaporation flux j and the corresponding heat flow Q as defined in Eqs. (7) and (8). The result depends on the bulk distribution of the vapor f_v, and in this section it is assumed that the vapor is in a Maxwellian distribution where the pressure differs from the liquid saturation pressure, $p_v \neq p_{sat}(T_l)$, and the temperatures of vapor and liquid are allowed to be different, $T_v \neq T_l$. This is the basic assumption of the classical Hertz-Knudsen theory, and for this reason we consider it here. In nonequilibrium between vapor and liquid one will expect temperature gradients in liquid and vapor, so that the Chapman-Enskog distribution (14) will be a more reasonable choice—it will be considered in the next section.

All computations are performed in a frame where the interface is at rest. The vapor has a net velocity $v = j/\rho_v$ with respect to the interface, and thus $C_z = c_z - j/\rho_v$ where c_z is the microscopic velocity of a particle relative to the interface and C_z the peculiar velocity, which is measured with respect to the rest frame of the vapor. This difference is ignored in the present section by setting $C_z = c_z$, so the results can be expected to be valid only for slow evaporation or condensation rates. Then, the vapor distribution function is given by

$$f_v = f_M(p_v, T_v) = \frac{p_v}{mRT_v}\frac{1}{\sqrt{2\pi RT_v}^3}\exp\left(-\frac{c^2}{2RT_v}\right). \quad (21)$$

The distribution of the specularly reflected molecules is identical to the incident distribution, except that the signs of the terms containing c_z are reversed. Since the Maxwellian (21) is quadratic in the velocity, reversing the sign of the velocity for the reflected distribution has no effect; thus, the distribution of specularly reflected particles is

$$f_{v\text{-}ref}(p_v, T_v) = f_M(p_v, T_v).$$

Under these assumptions, the distribution function of the vapor just at the interface is given by

$$f_{c_z>0} = \theta_c f_M(p_{sat}(T_l), T_l) + \gamma(1-\theta_c) f_M(p_v, T_v) + (1-\gamma)(1-\theta_c) f_M(p^*, T_l), \quad (22)$$

$$f_{c_z<0} = f_M(p_v, T_v).$$

This will now be used in Eqs. (7) and (8) to compute mass and energy flux over the interface.

The pressure p^* is computed from Eq. (16) which now becomes

$$-\frac{p_v}{\sqrt{2\pi RT_v}} + \frac{\gamma p_v}{\sqrt{2\pi RT_v}} + \frac{(1-\gamma)p^*}{\sqrt{2\pi RT_l}} = 0, \quad (23)$$

so that

$$p^* = p_v\sqrt{\frac{T_l}{T_v}}. \quad (24)$$

B. Evaporation and condensation mass flux

For the computation, the integral for j can be split into half-space integrals

$$j = \int mc_z f d\mathbf{c} = \int_{c_z\geqslant 0} mc_z f_{c_z>0} d\mathbf{c} + \int_{c_z\leqslant 0} mc_z f_{c_z<0} d\mathbf{c}. \quad (25)$$

After inserting (22), integration yields

$$j = \frac{1}{\sqrt{2\pi}}\left(\eta(T_l, T_l)\frac{p_{sat}(T_l)}{\sqrt{RT_l}} - \eta(T_l, T_v)\frac{p_v}{\sqrt{RT_v}}\right). \quad (26)$$

Here,

$$\eta(T_l, T) = \psi\left(1 - \frac{T_l\omega}{T_l + T}\right) \quad (27)$$

is a mean condensation and evaporation coefficient for mass. The mass evaporation coefficient is $\eta(T_l, T_l) = \psi(1-\omega/2)$, a constant which was already given in Ref. [17]. The mass condensation coefficient $\eta(T_l, T_v)$ depends on the temperatures of both the vapor and liquid. Note that the accommodation coefficient does not appear, since reflected particles do not take part in evaporation or condensation.

C. Energy flux

The computation of the energy flux (8) follows the same line: after splitting into two half-space integrals and inserting Eq. (2), integration yields

$$Q = \sqrt{\frac{2}{\pi}}[\varphi(T_l, T_l)p_{sat}(T_l)\sqrt{RT_l} - \varphi(T_l, T_v)p_v\sqrt{RT_v}], \quad (28)$$

where the mean condensation and evaporation coefficient for energy exchange at the interface is given by

$$\varphi(T_l, T) = \gamma\varphi_s(T_l, T) + (1-\gamma)\varphi_d(T_l, T), \quad (29)$$

with

$$\varphi_s(T_l, T) = \psi\left(1 - \omega\frac{(2T_l + T)T_l}{2(T_l + T)^2}\right) \quad (30)$$

and

$$\varphi_d(T_l, T) = 1 - \frac{1 - \psi\left(1 - \frac{3\omega}{8}\right)}{1 - \psi\left(1 - \frac{\omega}{2}\right)}\left[1 - \psi\left(1 - \omega\frac{T_l}{T + T_l}\right)\right]\frac{T_l}{T}. \quad (31)$$

Here, φ_s can be considered as a mean energy condensation coefficient for specularly reflected particles and φ_d as a mean energy condensation coefficient for diffusively reflected (thermalized) particles.

The equations above link the mean evaporation and condensation coefficients $\eta(T_l, T)$ and $\varphi(T_l, T)$ to the parameters ψ and ω that determine the condensation probability of a single vapor particle hitting the interface. From the above analysis follows that the mean evaporation coefficients $\eta(T_l, T_l)$ and $\varphi(T_l, T_l)$ are constants, while the mean condensation coefficients $\eta(T_l, T_v)$ and $\varphi(T_l, T_v)$ depend explicitly on the temperatures of vapor and liquid.

D. Constant condensation coefficients

The factor ω in Eq. (15) controls the temperature and velocity dependence of the condensation coefficient. Setting $\omega = 0$ yields the constant condensation coefficient $\theta_c = \psi$ and

$$j = \frac{\psi}{\sqrt{2\pi}}\left(\frac{p_{sat}(T_l)}{\sqrt{RT_l}} - \frac{p_v}{\sqrt{RT_v}}\right),$$

$$Q = \psi\sqrt{\frac{2}{\pi}}\left\{p_{sat}(T_l)\sqrt{RT_l} - \left[\gamma + \frac{1-\gamma}{\psi}\left(1 - (1-\psi)\frac{T_l}{T_v}\right)\right]p_v\sqrt{RT_v}\right\}. \quad (32)$$

For the special case $\psi = 1$ we recover the classical Hertz-Knudsen laws [5,6]

$$j = \frac{1}{\sqrt{2\pi}}\left(\frac{p_{sat}(T_l)}{\sqrt{RT_l}} - \frac{p_v}{\sqrt{RT_v}}\right),$$

$$Q = \sqrt{\frac{2}{\pi}}[p_{sat}(T_l)\sqrt{RT_l} - p_v\sqrt{RT_v}]. \tag{33}$$

Here we remark that for constant condensation and evaporation coefficients, one often finds the generalized Hertz-Knudsen equation written as [38,39]

$$j = \frac{1}{\sqrt{2\pi}}\left(\frac{\Theta_e p_{sat}(T_l)}{\sqrt{RT_l}} - \frac{\Theta_c p_v}{\sqrt{RT_v}}\right). \tag{34}$$

There is much debate regarding the values and dependences of Θ_c and Θ_e. Eames *et al.* [38] and Marek and Straub [39] reviewed the literature on condensation and evaporation coefficients of water and found that published values for both vary between 0.01 and 1. It is agreed upon that Θ_c and Θ_e are equal in equilibrium. If they are constants, then they must be equal also outside equilibrium to satisfy equilibrium conditions. That is, $j=Q=0$ for the equilibrium conditions $T_l = T_v = T$ and $p_v = p_{sat}(T)$ only if $\Theta_e = \Theta_c$.

Note that even for the constant evaporation coefficient $\Theta_c = \psi$, the condensation coefficient in the energy flux, $\varphi(T_l, T_v)$, depends on the temperatures as long as thermalization of reflected particles occurs—i.e., if $\gamma \neq 1$—while the corresponding coefficient $\eta(T_l, T_v)$ is constant. Thermalization implies an exchange of energy between vapor and liquid without an exchange of mass, and that leads to the temperature dependence of the heat transfer coefficient.

V. CHAPMAN-ENSKOG THEORY

A. Distribution function

In general, net evaporation or condensation occurs in nonequilibrium processes, where the vapor will not be in a Maxwellian distribution. As long as the vapor is not too rarefied, the Chapman-Enskog distribution (14) will give a good description of the bulk vapor; we shall consider it now for the computation of the interface fluxes.

As before, we consider a frame where the interface is at rest. We assume that the normal of the interface points into the z direction and that the vapor velocity $v_i = \{0, 0, v_z\}$ has no contribution parallel to the interface. Furthermore, we shall assume that the flow velocity v_z is relatively small and linearize in this quantity, so that the square of the peculiar velocity is

$$C^2 = c^2 - 2v_z c_z + v^2 \simeq c^2 - 2v_z c_z. \tag{35}$$

We substitute for the peculiar velocity into the Maxwellian (10) and perform a first-order Taylor expansion about zero in v_z to obtain the Maxwellian for a small mean vapor velocity:

$$f_{M\text{-}v} = \frac{p}{mRT}\frac{1}{\sqrt{2\pi RT^3}}\exp\left(-\frac{c^2}{2RT}\right)\left(1 + \frac{c_z v_z}{RT}\right). \tag{36}$$

Equation (36) is incorporated into the first-order CE distribution, Eq. (14), which for one-dimensionial problems can be written as

$$\begin{aligned} f_{CE\text{-}v} &= f_{M\text{-}v}\left(1 - \frac{2}{5}\frac{\kappa}{pR}c_z\left(\frac{c^2}{2RT} - \frac{5}{2}\right)\frac{1}{T}\frac{dT}{dz}\right) \\ &= \frac{p}{mRT}\frac{1}{\sqrt{2\pi RT^3}}\exp\left(-\frac{c^2}{2RT}\right) \\ &\quad\times\left[1 + \frac{c_z v_z}{RT} - \frac{2}{5}\frac{\kappa}{pR}c_z\left(\frac{c^2}{2RT} - \frac{5}{2}\right)\frac{1}{T}\frac{dT}{dz}\right], \end{aligned} \tag{37}$$

where second-order terms in v_z and dT/dz are ignored.

Integrating Eqs. (7) and (8) over full velocity space using Eq. (37) yields the bulk mass and energy flows as

$$j = \frac{p}{RT}v_z, \quad Q = \frac{5}{2}pv_z - \kappa\frac{dT}{dz}.$$

These can be used to rewrite the CE distribution as

$$\begin{aligned} f_{CE\text{-}v} &= \frac{p}{mRT}\frac{1}{\sqrt{2\pi RT^3}}\exp\left(-\frac{c^2}{2RT}\right) \\ &\quad\times\left[1 - \frac{j}{p}\left(\frac{c^2}{2RT} - \frac{7}{2}\right)c_z + \frac{2}{5}\frac{Q}{pRT}\left(\frac{c^2}{2RT} - \frac{5}{2}\right)c_z\right]. \end{aligned} \tag{38}$$

This distribution will be used to represent the bulk vapor and the distribution of condensing particles.

The distribution of the specularly reflected particles is given by

$$\begin{aligned} f_{CE\text{-}v\text{-}ref} &= \frac{p}{mRT}\frac{1}{\sqrt{2\pi RT^3}}\exp\left(-\frac{c^2}{2RT}\right) \\ &\quad\times\left[1 + \frac{j}{p}\left(\frac{c^2}{2RT} - \frac{7}{2}\right)c_z - \frac{2}{5}\frac{Q}{pRT}\left(\frac{c^2}{2RT} - \frac{5}{2}\right)c_z\right]. \end{aligned}$$

Note that the signs of the terms containing c_z have changed from the incident distribution (38).

The evaporating molecules are again described by the equilibrium Maxwellian distribution, Eqs. (10) and (20). The mean velocity of the evaporating molecules is assumed to be equal to the velocity of the liquid at the interface. Due to mass conservation, $v_l\rho_l = v_v\rho_v = j$, and since the liquid density is much greater than the vapor density, $\rho_l \gg \rho_v$, it follows that $v_l \ll v_v$. Since the vapor velocity is assumed to be small, the liquid velocity is negligible. It follows that the evaporating distribution can be approximated by the equilibrium Maxwellian with $C=c$, as in the Hertz-Knudsen approach presented earlier.

The interface distribution is then given as

$$\begin{aligned} f_{c_z>0} &= \theta_c f_M(p_{sat}(T_l), T_l) + \gamma(1-\theta_c)f_{CE\text{-}v\text{-}ref}(p_v, T_v) \\ &\quad + (1-\gamma)(1-\theta_c)f_M(p^*, T_l), \\ f_{c_z<0} &= f_{CE\text{-}v}(p_v, T_v), \end{aligned} \tag{39}$$

where, again, the pressure p^* follows from Eq. (16).

B. Mass and energy flux

Tedious manipulations reveal that the fluxes of mass and energy at the interface are given by

$$j = \frac{1}{\sqrt{2\pi}}\left([\mathcal{R}_{11}^{-1}\eta(T_l,T_l) + 2\mathcal{R}_{12}^{-1}\varphi(T_l,T_l)RT_l]\frac{p_{sat}(T_l)}{\sqrt{RT_l}} - [\mathcal{R}_{11}^{-1}\eta(T_l,T_v) + 2\mathcal{R}_{12}^{-1}\varphi(T_l,T_v)RT_v]\frac{p_v}{\sqrt{RT_v}}\right),$$

$$Q = \sqrt{\frac{2}{\pi}}\left(\left[\frac{\mathcal{R}_{21}^{-1}}{2RT_l}\eta(T_l,T_l) + \mathcal{R}_{22}^{-1}\varphi(T_l,T_l) \right] p_{sat}(T_l)\sqrt{RT_l} - \left[\frac{\mathcal{R}_{21}^{-1}}{2RT_v}\eta(T_l,T_v) + \mathcal{R}_{22}^{-1}\varphi(T_l,T_v) \right] p_v\sqrt{RT_v}\right), \tag{40}$$

where $\mathcal{R}_{\alpha\beta}^{-1}$ are the elements of the inverse of the matrix $\mathcal{R}$:

$$\mathcal{R}_{11} = \frac{2-\psi}{2} + \frac{\psi\omega}{2}\frac{T_l^{3/2}\left(T_l + \frac{5}{2}T_v\right)}{(T_l+T_v)^{5/2}},$$

$$\mathcal{R}_{12} = -\frac{3}{10}\frac{\psi\omega}{R}\frac{T_l^{3/2}}{(T_l+T_v)^{5/2}},$$

$$\mathcal{R}_{21} = (1-\gamma)\frac{1-\psi(1-3\omega/8)}{1-\psi(1-\omega/2)} \times \left[1-\psi+\psi\omega\left(T_l+\frac{5}{2}T_v\right)\frac{T_l^{3/2}}{(T_l+T_v)^{5/2}} \right] RT_l + \frac{1}{8}\gamma\psi\omega\frac{T_l^{3/2}(21T_vT_l+6T_v^2)}{(T_l+T_v)^{7/2}}RT_v,$$

$$\mathcal{R}_{22} = \frac{1+\gamma(1-\psi)}{2} - \frac{3}{5}\psi\omega\left(1-\frac{1}{8}\frac{\psi\omega(1-\gamma)}{1+\psi(\omega/2-1)}\right)\frac{T_l^{5/2}}{(T_l+T_v)^{5/2}} + \frac{\gamma\psi\omega}{20}\frac{T_l^{3/2}(22T_l^2+5T_vT_l-2T_v^2)}{(T_l+T_v)^{7/2}}.$$

Comparison with Eqs. (26) and (28) indicates that for the Maxwellian case $\mathcal{R}_{11}^{-1}=\mathcal{R}_{22}^{-1}=1$ and $\mathcal{R}_{12}^{-1}=\mathcal{R}_{21}^{-1}=0$, so that in this case $\mathcal{R}$ is the unit matrix.

The factors in the square brackets in Eqs. (40) are the mean evaporation and condensation coefficients. It is evident that they are complicated functions of the temperatures T_l, T_v and the coefficients γ, ω, ψ, but we shall not give the explicit expressions. Instead, we consider some special cases for the parameters.

C. Constant condensation coefficients

1. All vapor particles condense: $\omega=0$ and $\psi=1$

The most common assumption in the literature is that all vapor particles that hit the interface condense; this corresponds to setting $\theta_c=1$—that is, $\omega=0$ and $\psi=1$. For this case, mass and energy fluxes are twice as large as for the classical Hertz-Knudsen theory (33)—i.e. [1,40],

$$j = 2\frac{1}{\sqrt{2\pi}}\left(\frac{p_{sat}(T_l)}{\sqrt{RT_l}} - \frac{p_v}{\sqrt{RT_v}}\right),$$

$$Q = 2\sqrt{\frac{2}{\pi}}(p_{sat}(T_l)\sqrt{RT_l} - p_v\sqrt{RT_v}). \tag{41}$$

2. Condensation probability independent of impact energy: $\omega=0$ and $\psi\neq 1$

This case assumes that all vapor particles have the same likelihood for condensation, irrespective of their energy, and allows for diffuse and specular reflection. In this case, the evaporation and condensation mass flux is given by

$$j = \frac{2\psi}{2-\psi}\frac{1}{\sqrt{2\pi}}\left(\frac{p_{sat}(T_l)}{\sqrt{RT_l}} - \frac{p_v}{\sqrt{RT_v}}\right) \tag{42}$$

and the corresponding energy flux is

$$Q = \sqrt{\frac{2}{\pi}}\left(\frac{2\psi}{2-\psi}p_{sat}(T_l)\sqrt{RT_l} - \left[\frac{(1-\gamma+\gamma\psi)(2-\psi)}{\psi[1+\gamma(1-\psi)]} - \frac{2(1-\gamma)(1-\psi)}{\psi[1+\gamma(1-\psi)]}\frac{T_l}{T_v}\right]p_v\sqrt{RT_v}\right). \tag{43}$$

The mass flux does not depend on the number of specularly reflected particles, as can be seen from its independence from γ, but the energy flux depends on γ. This reflects the fact that thermalized vapor particles exchange energy with the liquid, while specularly reflected particles only exchange momentum.

If all particles that do not condense are specularly reflected, we have $\gamma=1$ and the energy flux reduces further to

$$Q = \frac{2\psi}{2-\psi}\sqrt{\frac{2}{\pi}}[p_{sat}(T_l)\sqrt{RT_l} - p_v\sqrt{RT_v}]. \tag{44}$$

For the special case that all noncondensing particles are thermalized, $\gamma=0$, we obtain instead

$$Q = \frac{2\psi}{2-\psi}\sqrt{\frac{2}{\pi}}\left(p_{sat}(T_l)\sqrt{RT_l} - \left[\frac{2T_l-T_v}{T_v} + \frac{2}{\psi}\frac{T_v-T_l}{T_v}\right]p_v\sqrt{RT_v}\right). \tag{45}$$

Note that all cases discussed here fulfill the equilibrium conditions—that is, $j=Q=0$ if $T_l=T_v=T$ and $p_v=p_{sat}(T)$.

Equation (42) for the mass flow is due to Schrage [1]; see also [40]. Ytrehus [41], through comparison with the Bhatnager-Gross-Krook-Welander model equation and DSMC simulations, finds that the Hertz-Knudsen (HK) mass flux (33) underestimates the mass flux by an approximate factor of 2. He also observes that the Schrage expression (42) leads to a slightly overestimated mass flux, likely due to neglect of collisional effects in the Knudsen layer.

D. A remark on momentum flux

The momentum flux per unit area normal to the interface is given by

$$P_{zz} = \int_{-\infty}^{\infty} mc_z^2 f d\mathbf{c}.$$

When evaluated in the bulk vapor, where the distribution is given by Eq. (37)—i.e., under omission of quadratic terms and shear stress effects—this yields

$$P_{zz|\text{bulk}} = p_v.$$

When computed with the interface distribution (39), $P_{zz|\text{interface}}$ is different from the bulk value, with an expression that is not shown here. Barrett and Clement [40] argue that this discrepancy between normal force at interface and in the bulk implies the violation of the conservation law for momentum which states that P_{zz} must be a constant. The explanation for this problem lies in the fact that (a) we omitted anisotropic stresses in the distribution function $f_{CE\text{-}v}$ and (b) we ignored the Knudsen layer. In particular, one can expect that the difference between the bulk and interface values, $P_{zz|\text{interface}} - P_{zz|\text{bulk}}$, would vanish exponentially over the Knudsen layer—that is, within the distance of few mean free paths away from the interface—if Knudsen layer effects were accounted for. In our treatment, the Knudsen layer is reduced to zero thickness, which results in a jump for P_{zz}.

In order to discuss the importance of this jump in the momentum flux, we computed the relative error $1 - P_{zz|\text{interface}}/P_{zz|\text{bulk}}$ for random values of the parameters within their range of definition as suggested by the Toronto experiments—viz., $\omega \in [0,1]$, $\psi \in [0,1]$, $\gamma \in [0,1]$, $T_l, T_v \in [273\ \text{K}, 313\ \text{K}]$, and $p_v, p_{sat} \in [0.611\ \text{kPa}, 10\ \text{kPa}]$. We found an average relative error of $\sim 0.6\%$ based on 10^5 sample calculations. It follows that the error is not significant, and thus the simplifying assumptions are justified.

Note that Barrett and Clement's discussion is based on the so-called Schrage distribution at the interface [40], which results from setting $Q=0$ in Eq. (38). For this case they point out problems with the energy flux as well, which we believe are due to not having the energy flux in the distribution function. Since we use the Chapman-Enskog distribution (38) with the energy flux, this criticism does not apply.

VI. PHENOMENOLOGICAL THEORIES

A. Thermodynamic of irreversible processes

For reasons of comparison, we briefly discuss simple phenomenological laws for the evaporation mass and energy fluxes, which are based on the concepts of thermodynamics of irreversible processes [19].

The balances of energy and entropy at the interface read

$$jh_l + q_l = jh_v + q_v, \tag{46}$$

$$\sigma = j(s_v - s_l) + \frac{q_v}{T_v} - \frac{q_l}{T_l} \geqslant 0, \tag{47}$$

where q_l, q_v are the nonconvective energy fluxes in liquid and vapor, respectively, and σ is the entropy generation rate due to evaporation or condensation. These two equations can be combined to give

$$\sigma = j\left[\frac{g_l}{T_l} - \frac{g_v}{T_v} + h_v\left(\frac{1}{T_v} - \frac{1}{T_l}\right)\right] + q_v\left(\frac{1}{T_v} - \frac{1}{T_l}\right) \geqslant 0, \tag{48}$$

where $g = h - Ts$ is the Gibbs free energy.

We follow the ideas of classical TIP and write the entropy production σ as a sum of products of "thermodynamic fluxes" J_A and "thermodynamic forces" F_A,

$$\sigma = \sum_A J_A F_A,$$

where, in our case,

$$J_A = \{j, q_v\}, \quad F_A = \left\{\frac{g_l}{T_l} - \frac{g_v}{T_v} + h_v\left(\frac{1}{T_v} - \frac{1}{T_l}\right), \frac{1}{T_v} - \frac{1}{T_l}\right\}. \tag{49}$$

Positivity of the entropy production is guaranteed by a linear "phenomenological ansatz"

$$J_A \sum_B A_{AB} F_B,$$

where the matrix A_{AB} must be positive definite.

The choice of fluxes and forces is not unique, and a linear transformation $\hat{X}_{AB}$ can be used to define new fluxes and forces according to $\hat{J}_B = J_A \hat{X}_{AB}$, $\hat{F}_B = \hat{X}_{BC}^{-1} F_C$, while $\sigma = J_A F_A = \hat{J}_B \hat{F}_B$. The phenomenological laws for the transformed quantities read $\hat{J}_A = \hat{A}_{AB} \hat{F}_B$, with the corresponding matrix of phenomenological coefficients given as $\hat{A}_{AB} = \hat{X}_{AC}^T A_{CD} \hat{X}_{DB}$. According to the Onsager symmetry relations [19], there is one choice of forces and fluxes, $\tilde{J}_A$ and $\tilde{F}_A$, so that the corresponding matrix of phenomenological coefficients $\tilde{A}_{AB}$ is symmetric. This in turn implies that the matrix of phenomenological coefficients can be diagonalized, that is there is a transformation $\bar{X}_{AB}$ so that the corresponding fluxes and forces $\bar{J}_A, \bar{F}_A$ are related by a diagonal matrix $\tilde{A}_{AB} = \lambda_A \delta_{AB}$ (no summation over index A). Only detailed measurements can reveal the values of the phenomenological coefficients A_{AB}.

In this paper, we are mainly concerned with the models derived from kinetic theory, and we wish to consider a TIP-based model mainly for comparison. Therefore we choose the simplest approach, in which the matrix A_{AB} is a diagonal matrix, so that

$$j = \beta\left[\frac{g_l}{T_l} - \frac{g_v}{T_v} + h_v\left(\frac{1}{T_v} - \frac{1}{T_l}\right)\right], \tag{50}$$

$$q_v = \alpha\left(\frac{1}{T_v} - \frac{1}{T_l}\right). \tag{51}$$

β and α are the phenomenological coefficients, which must be non-negative to ensure non-negative entropy production. While this simple model gives results in good agreement to the experiments, we wish to emphasize that a detailed study of the Toronto experiments based on TIP should account for a completely filled matrix A_{AB}, including the nondiagonal elements, which describe the cross coupling of fluxes and

forces. As will be seen, the simulation results depend strongly on the geometry of the experiments. With the simple choice above, we can reproduce the general trends of the experiment, and only an exact simulation of the experiment—including its geometry—could be used to exactly determine the values of the coefficients A_{AB}.

Equation (51) implies that the heat flow from the interface into the vapor is solely driven by the temperature difference between liquid and vapor. Since Eq. (46) gives $q_l = q_v + j(h_v - h_l)$, this also implies that the heat of evaporation $j(h_v - h_l)$ is absorbed from (in the condensation case) or provided by (for evaporation) the liquid. This is plausible, since the heat conductivity of the liquid is substantially larger than the heat conductivity of the vapor.

We remark also that the heat flux in the bulk vapor is of course given by Fourier's law (12), while expression (51) is valid only at the interface.

For equilibrium where $g_l = g_v$ and $T_l = T_v$, we see that Eqs. (50) and (51) reduce to $j = 0$ and $q_v = 0$ (which implies $Q = 0$), satisfying the equilibrium conditions.

B. Statistical rate theory

Ward and Fang [23] used statistical rate theory to find an expression for the interface mass flux,

$$j = k_s \left\{ \exp\left[\frac{g_l}{RT_l} - \frac{g_v}{RT_v} + \frac{h_v}{R}\left(\frac{1}{T_v} - \frac{1}{T_l} \right) \right] - \exp\left[\frac{-g_l}{RT_l} + \frac{g_v}{RT_v} - \frac{h_v}{R}\left(\frac{1}{T_v} - \frac{1}{T_l} \right) \right] \right\}, \tag{52}$$

where the two terms are the evaporation and condensation rates, respectively. The coefficient k_s is given as

$$k_s = \frac{\vartheta p_{sat}(T_l)}{\sqrt{2\pi R T_l}}, \quad \vartheta = \exp\left\{ \frac{v_l(T_l)}{RT_l}[p_l - p_{sat}(T_l)] \right\},$$

where $p_l \simeq p_v$ is the liquid pressure at the interface. Note that we have changed the units (from molecular to mass units) in these expressions, to adjust them to the other equations. v_l denotes the specific volume of the liquid. For water in our range of study, $T_l \approx 298$ K, and $v_l \approx 10^{-3}$ m^3/kg; we estimate $v_l(T_l)/RT_l \approx 10^{-8}$ m^2/N. The difference between p_l^e and $p_{sat}(T_l)$ is small, thus $\vartheta \approx 1$, and the factor in front of the exponential reduces to

$$k_s = \frac{p_{sat}(T_l)}{\sqrt{2\pi R T_l}}. \tag{53}$$

Here k_s is just the first term of the HK mass flux (33) which assumes that all vapor particles that hit the interface condense. Thus, the same assumption is present in the SRT expression [23].

When we assume that the arguments in the exponentials are small, the SRT mass flux can be linearized to give

$$j = \frac{2k_s}{R}\left[\frac{g_l}{T_l} - \frac{g_v}{T_v} + h_v\left(\frac{1}{T_v} - \frac{1}{T_l} \right) \right]. \tag{54}$$

This is identical to the mass flux expression of TIP (50) when we identify

$$\beta = \beta_{SRT} = \frac{p_{sat}(T_l)}{R}\sqrt{\frac{2}{\pi R T_l}}. \tag{55}$$

Ward and Fang [23] do not provide an expression for the energy flux. However, in order to completely solve the balance laws for evaporation and condensation problems, an expression for the heat flux is indispensable. The above analysis shows that the SRT mass flux is essentially a nonlinear form of Eq. (50), and we suggest that the energy flux (51) can be used as a substitute in the absence of an SRT energy flux expression. It would be interesting to use SRT to find a nonlinear expression for Q, but this is outside the scope of our work.

Finally we comment that the values of the phenomenological coefficients A_{AB} or—in our simplified theory—α and β are not constants, but will depend on the local conditions, in particular on the temperatures T_l and T_v and on the pressure p_v. Thus, the coefficients must be determined by fitting to measured data. Since the SRT expression β_{SRT} follows from the assumption that all vapor particles condense—i.e., a condensation coefficient of $\theta_c = 1$—one can introduce the condensation coefficient here by setting $\beta = \theta_c \beta_{SRT}$ and fit θ_c and α to the experiments.

VII. EVAPORATION AND CONDENSATION EXPERIMENTS

A. Toronto experiments

To test our models, we shall aim at simulating the experiments by Ward, Fang, and Stanga [2–4], who studied liquid evaporating from or condensing to its own vapor. Figure 2 shows their apparatus [4].

Water was supplied through the bottom of the funnel by a syringe pump and withdrawn as vapor from the top of the chamber. Steady-state evaporation was achieved by adjusting the rate of liquid water entry at the inlet and regulating the vapor pressure by opening and closing a vacuum valve in line with a vacuum pump.

For condensation, the syringe pump withdrew water at a constant rate and the water exiting the funnel was cooled by a cooling jacket causing the water vapor in the chamber to condense. Steady state was maintained by allowing water to evaporate from the test liquid reservoir to replace the water condensing into the funnel.

The evaporation and condensation rates were measured based on the syringe pump rate. The vapor pressure was measured with a mercury manometer. Temperatures in the liquid and vapor were measured along the center line with thermocouples, which were located using a positioning micrometer. The liquid vapor interface position and radius of curvature were established by observation using a cathetometer. Temperatures were measured in the vapor within one to five mean free paths of the interface. Temperatures in the liquid were measured within 0.25 mm of the interface.

The apparatus was radially symmetric. The liquid vapor interface at the top of the funnel was assumed to be hemispherical. Ward, Fang, and Stanga suggest there is very little heat transfer with, or through the walls of the funnel.

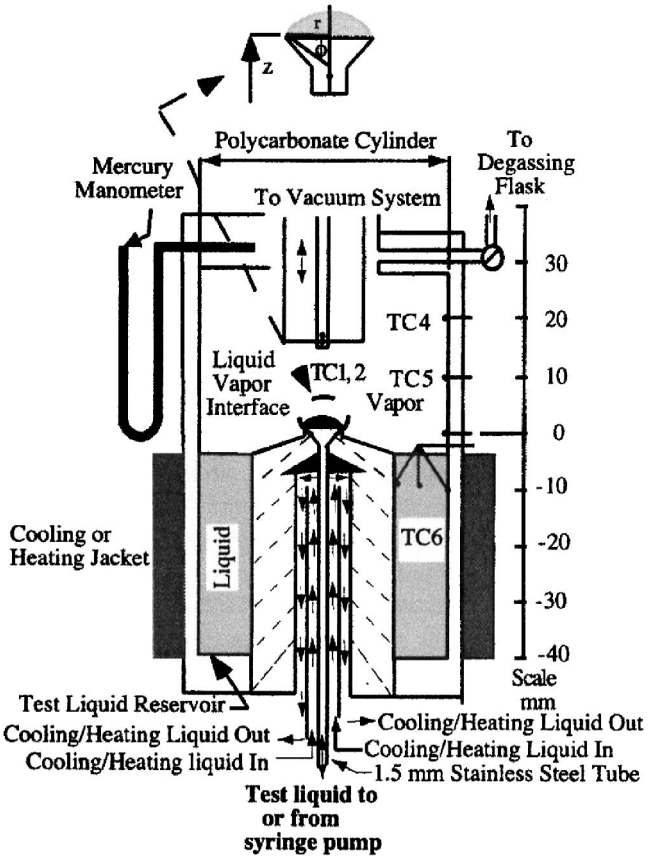

FIG. 2. Setup of the Toronto steady-state evaporation experiment [4].

For evaporation Fang and Ward [2,3], T_v was as much as 7.8°C higher than the liquid interface temperature T_l. Ward and Stanga [4] observed $T_v > T_l$ also for condensation, but with smaller jumps. They observed the same vapor temperature gradient direction in condensation as for evaporation [4].

Table I gives the values of a typical experiment, where T_{bl} and T_{bv} are the boundary temperatures of liquid and vapor, L_l and L_v are the distance between interface and boundaries for liquid and vapor, and T_l and T_v denote the temperatures of liquid and vapor directly at the interface.

As becomes clear from Fig. 2, the experiment takes place in a three-dimensional setting. In the following, we shall try to mimic the main features of the experiments by considering simpler geometries. Since it turned out that geometrical effects play an important role, we consider planar and spherical one-dimensional settings.

B. One-dimensional planar interface geometry

Figure 3 describes the basic geometry of the one-dimensional (1D) planar setting. All fluxes and gradients are assumed to be perpendicular to the liquid vapor interface, which is a plane. The one-dimensional mass flux per unit area j and the energy flux per unit area Q are defined as positive in the positive z direction, the direction of evaporation. At the interface, $z=0$, the liquid temperature is T_l and the vapor temperature is T_v.

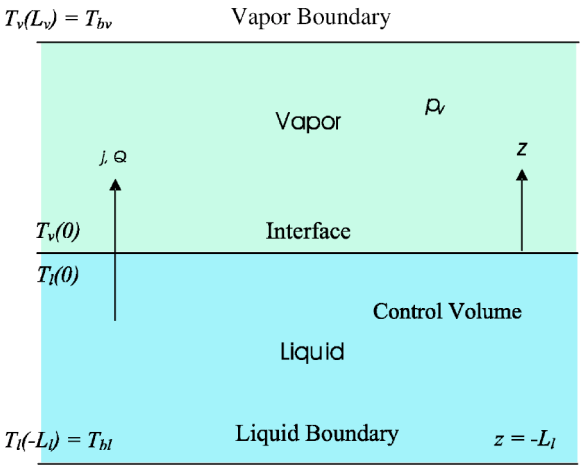

FIG. 3. Geometry of the planar setting.

The liquid and vapor boundary temperatures are specified such that at the liquid boundary $z=-L_l$ the liquid temperature is T_{bl}, and at the vapor boundary $z=L_v$, the vapor temperature is T_{bv}. Furthermore, the pressure in the vapor p_v is controlled—e.g., by a pump.

Mass and energy flow either when a temperature gradient is imposed across the system, $T_{bl} \neq T_{bv}$, or by perturbing the vapor pressure p_v away from the saturation pressure $p_{sat}(T)$. For equal boundary temperatures $T_{bl}=T_{bv}=T_b$, a vapor pressure below the saturation pressure $p_v < p_{sat}(T_b)$ will cause a net evaporation, while $p_v > p_{sat}(T_b)$ will cause a net condensation.

Note that, in accordance with the Toronto experiments, interface and boundaries remain at fixed locations, which implies that mass is transported over the boundaries.

C. Balance equations

We first consider the bulk fluids away from the interface. The balance of mass [42] for one-dimensional steady state reduces to

$$\frac{\partial \rho v_z}{\partial z} = 0, \tag{56}$$

where z represents the vertical direction; see Fig. 3. Equation (56) implies that the mass flux $j=\rho v_z$ is constant with posi-

TABLE I. Evaporation experiment E1 data of Ward *et al.* [4].

Prescribed data					Measured data			
p_v (Pa)	L_l (mm)	L_v (mm)	T_{bl} (°C)	T_{bv} (°C)	T_l (°C)	T_v (°C)	ΔT	j (kg/m^2 s)
593	4.970	18.590	26.060	25.710	−0.4	2.6	3.0	1.017×10^{-3}

tion everywhere in the domain. Moreover, since no mass is accumulated at the interface, the mass flow from the liquid into the interface must be equal to the mass flow from the interface to the vapor, so that

$$j = \rho_l v_l = \rho_v v_v = \text{const}, \tag{57}$$

where the index l refers to the liquid and the index v refers to the vapor. The value of j directly at the interface must be computed from the interface conditions presented above, and j has the same constant value throughout the domain.

The conservation of energy [42] in differential form for one-dimensional steady state processes reads

$$\frac{\partial}{\partial z}\left[\rho\left(u+\frac{v^2}{2}\right)v_z + p_{zz}v_z + q_z\right] = \rho F_z v_z. \tag{58}$$

Here, u is the internal energy and $q_z = -\kappa\,\partial T/\partial z$ is the conductive heat flux. Again, we neglect the kinetic energy term $v^2/2$, since it will be insignificant relative to the internal energy as long as the evaporation rate is small, which is the case if the evaporation Mach number $\mathrm{Ma} = v/\sqrt{(c_p/c_v)RT}$ is not larger than 0.1. Moreover, we neglect gravitational effects, which play no role for this process (apart from keeping the denser liquid below the vapor), and assume isotropic pressure and no shear forces, so that $p_{ij} = p\delta_{ij}$. Under these assumptions the one-dimensional steady-state energy balance reduces to

$$\frac{\partial}{\partial z}\left[\rho h v_z - \kappa\frac{dT}{dz}\right] = 0,$$

where $h = u + p/\rho$ denotes specific enthalpy. Like the balance of mass this reduces to constant liquid and vapor total energy fluxes,

$$Q = jh_l - \kappa_l\frac{dT}{dz} = jh_v - \kappa_v\frac{dT}{dz} = \text{const}. \tag{59}$$

The value of Q directly at the interface must be computed from the interface conditions presented above, and Q has the same constant value throughout the domain. The (differential) equations (57) and (59) must be solved together with the interface conditions to find the values of the fluxes j and Q, as well as the temperature profiles in vapor and liquid, and the temperature jump at the interface.

Before we proceed with the solution, we briefly show that, under our assumptions, pressure gradients can be ignored. The momentum balance in for steady state in the one-dimensional setting reads [42]

$$\frac{\partial p + \rho v_z v_z}{\partial z} = \rho g, \tag{60}$$

where we again used $p_{ij} = p\delta_{ij}$. As before, we can ignore the square of the velocity if the Mach number is small. Moreover, due to the low density of the vapor, the gravitational force can be ignored as well, so that the pressure in the vapor is constant throughout the domain,

$$\frac{\partial p_v}{\partial z} = 0. \tag{61}$$

In particular, the pressure of the vapor directly at the interface is equal to the pressure prescribed at the boundary.

D. Constitutive assumptions

In order to solve the boundary value problem, constitutive equations for enthalpies, heat flux, and saturation pressure are required. We consider these under the simplifying assumptions that the liquid is incompressible and the vapor an ideal gas with constant specific heats. Since the Toronto experiments were performed with water, we shall consider the values for water, with exception of the vapor heat capacity: Since we considered the evaporation and condensation rates for a monatomic gas we need to be consistent and consider the specific heat for monatomic molecules

$$c_p = \frac{5}{2}R = 1.15\ \text{kJ/(kg K)}, \tag{62}$$

where $R = 0.462\ \text{kJ/(kg K)}$ is the gas constant of water.

For the liquid we have enthalpy and entropy given by

$$h_l = c_l(T - T_0)\ ,\ s_l = c_l \ln\frac{T}{T_0}, \tag{63}$$

where $c_l = 4.18\ \text{kJ/(kg K)}$ is the specific heat and $T_0 = 298\ \text{K}$ is a reference temperature. Note that for an incompressible liquid the enthalpy has an additional term $(1/\rho_l)\times(p_l - p_0)$, which, however, can be ignored for smaller deviations from the reference pressure $p_0 = p_{sat}(298\ \text{K}) = 3.169\ \text{kPa}$ due to the large mass density ρ_l.

Under the assumption that the specific heat c_p of the vapor is constant, vapor enthalpy and entropy are given as

$$h_v = c_p(T - T_0) + \Delta h_0\ ,\ s_v = c_p \ln\frac{T}{T_0} - R\ln\frac{p}{p_0} + \frac{\Delta h_0}{T_0}, \tag{64}$$

with the enthalpy of vaporization $\Delta h_0 = 2442.3\ \text{kJ/kg}$ at T_0. This choice ensures that at the reference temperature the heat of evaporation $h_v - h_l = T_0(s_v - s_l)$ has its proper value. In general we have for the heat of evaporation (for $T_v = T_l = T$ at the interface) $h_v - h_l = \Delta h_0 - (c_l - c_p)(T - T_0)$ which gives a reasonable approximation for small deviations from the temperature T_0.

The saturation pressure $p_{sat}(T)$ is the equilibrium pressure of a fluid at temperature T that exists simultaneously in both liquid and vapor phases, with the well-known equilibrium conditions

$$p = p_v = p_l = p_{sat}(T),\ T = T_v = T_l,\ g_l = g_v. \tag{65}$$

With the above relations for enthalpy and entropy and $g = h - Ts$, the last condition can be solved for saturation pressure,

$$p_{sat}(T) = p_0 \exp\left\{ \frac{c_l - c_p}{R}\left[1 - \frac{T_0}{T} - \ln\left(\frac{T}{T_0}\right)\right] + \frac{\Delta h_0}{R}\left(\frac{1}{T_0} - \frac{1}{T}\right)\right\}. \quad (66)$$

The saturation pressure computed from this equation matches well with tabulated data for temperatures between 273 K and 373 K (despite the error in the specific heat of the vapor).

Finally, we assume that the heat conductivities of liquid and vapor are constants, which we also chose for water at 298 K. Then we have $\kappa_l = 0.55$ W/m K and $\kappa_v = 1.4 \times 10^{-2}$ W/m K [43].

The actual values of the coefficients c_l, c_p, κ_l, κ_v, etc., are not constant, but depend on the local temperature. We did some studies for the importance of the temperature dependence for the results [44], which showed that influence of the temperature variation is reasonably small, so that the assumption of constant parameters is well justified.

E. Reference adjustment

The vapor enthalpy used in our kinetic-theory-based equations differs from the vapor enthalpy (65), since both are based on different reference values. Indeed, in kinetic theory the enthalpy is given by $h_{v|\mathrm{kt}} = c_p T$ which gives a difference $h_{v|\mathrm{kt}} - h_v = c_p T_0 - \Delta h_0$.

In order to compensate for this difference, the total energy flux Q_{kt} as computed from kinetic theory must be corrected by adding the portion of convective energy flow due to the different reference enthalpies, which yields

$$Q = Q_{\mathrm{kt}} + j(\Delta h_0 - c_p T_0). \quad (67)$$

At first glance it seems that the change of the reference state influences the expression for the entropy generation (47) and (48) or the thermodynamic forces (49). However, a closer look on Eq. (47) reveals that the entropy generation rate depends only on the difference $s_v - s_l$ and the nonconvective fluxes q_l and q_v, and is therefore independent of the chosen reference. Also the thermodynamic forces (49) are independent from the chosen reference, since they can be written as

$$F_A = \left\{ s_v - s_l - \frac{h_v - h_l}{T_l}, \frac{1}{T_v} - \frac{1}{T_l}\right\}. \quad (68)$$

This in turn implies that the phenomenological laws for the fluxes $J_A = \{j, q_v\}$, which were given as $J_A = \Sigma A_{AB} F_B$, are not affected by a change in the reference states for enthalpy or entropy. Indeed, only the total energy flux Q is affected, since the convective energy transport jh changes.

F. Liquid and vapor temperature profiles

After inserting the relations for enthalpy, Eqs. (63) and (64), the energy balance, Eq. (59), can be written as

$$\begin{aligned} jc_l(T_l(z) - T_0) - \kappa_l \frac{dT_l(z)}{dz} &= j[c_p(T_v(z) - T_0) + \Delta h_0] - \kappa_v \frac{dT_v(z)}{dz} \\ &= Q. \end{aligned} \quad (69)$$

These are two differential equations for the temperature in liquid and vapor, respectively. Note that, by Eqs. (57) and (59), Q and j are constants. Solution by using the variation of parameters and the boundary conditions for temperature yields

$$T_l(z) = T_{cl} + (T_{bl} - T_{cl})\exp\left(\frac{z + L_l}{a_l}\right), \quad (70)$$

$$T_v(z) = T_{cv} + (T_{bv} - T_{cv})\exp\left(\frac{z - L_v}{a_v}\right). \quad (71)$$

Here, we have introduced the constants

$$T_{cl} = \frac{Q}{jc_l} + T_0\ ,\ a_l = \frac{\kappa_l}{jc_l} \quad (72)$$

and

$$T_{cv} = \frac{Q}{jc_p} + T_0 - \frac{\Delta h_0}{c_p}\ ,\ a_v = \frac{\kappa_v}{jc_p}. \quad (73)$$

The temperatures T_l and T_v directly at the interface, where $z = 0$, are

$$T_l = T_{cl} + (T_{bl} - T_{cl})\exp\left(\frac{L_l}{a_l}\right), \quad (74)$$

$$T_v = T_{cv} + (T_{bv} - T_{cv})\exp\left(\frac{-L_v}{a_v}\right). \quad (75)$$

By Eqs. (72) and (73), the constants T_{cl} and T_{cv} depend on the values of the interface fluxes, j and Q, which in turn are functions of the temperatures T_l and T_v directly at the interface, as computed in Secs. IV and V,

$$j = \mathcal{J}(T_l, T_v), \quad Q = \mathcal{Q}(T_l, T_v). \quad (76)$$

The last four equations (74)–(76) therefore form a nonlinear set of equations for the four constants T_l, T_v, j, and Q. The four equations were solved simultaneously using the "FindRoot" function in Mathematica 4.1, which uses Newton's method with an initial guess to converge to an accuracy of six digits [45]. We made initial guesses for the two interface temperatures and fluxes, based on trial and error and knowledge of the equilibrium position. If these guesses are sufficiently close to the solution, then Newton's method will converge to a solution. There is no guarantee that there is only one solution, and it is possible that different solutions might be found with different initial guesses. However, we discount the possibility of multiple solutions for our system of equations for two reasons: the solutions we found appear to be realistic and agree well with measured data, and variation of the initial guesses did not alter the converged solution.

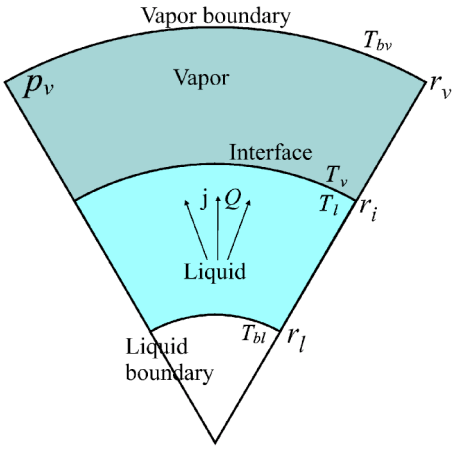

FIG. 4. Spherical model geometry.

Should the initial guess be too far from the solution and sufficient convergence is not achieved, an error message of nonconvergence is displayed.

G. Spherical geometry

We also consider the evaporation and condensation problem in spherical geometry (see Fig. 4) since we believe that the results of the Toronto experiment depend on geometry and can be better described in spherical geometry.

The boundary conditions are chosen as follows: the liquid boundary temperature T_{bl} is maintained at radius r_l, the liquid-vapor interface is at r_i, and the vapor boundary temperature T_{bl} is maintained at r_v. Moreover, the pressure of the vapor p_v is controlled by pumping vapor in or out at the outer boundary, and the location of the interface is kept constant by supplying or withdrawing liquid at r_l.

The temperatures of liquid and vapor interface are T_l and T_v, respectively, and mass flux and energy fluxes at the interface are denoted as j_i and Q_i. The radial fluxes and gradients are defined as positive for the outward direction, and we assume only radial fluxes, gradients, and jumps.

In steady state, the mass flux through each shell of constant radius must be the same, so that

$$j_r(r)r^2 = j_i r_i^2 = \text{const}. \tag{77}$$

Also the total energy flux through each shell must be the same, so that

$$Q_r(r)r^2 = Q_i r_i^2 = \text{const}. \tag{78}$$

The energy flux per unit area is now given by

$$Q_r = j_r h + q_r = \frac{j_i r_i^2}{r^2} h - \kappa \frac{dT(r)}{dr}. \tag{79}$$

Combining the last two equations yields a differential equation for temperature which must be solved for the vapor and the liquid. For the temperature in the vapor one finds

$$T_v(r) = T_{cv} + (T_{bv} - T_{cv}) \exp\left(\frac{r - r_v}{r r_v a_v}\right), \tag{80}$$

with the constants

$$T_{cv} = \frac{Q_i}{j_i c_p} + T_0 - \frac{\Delta h_0}{c_p}, \quad a_v = \frac{\kappa_v}{j_i r_i^2 c_p}. \tag{81}$$

The results for the liquid reads

$$T_l(r) = T_{cl} + (T_{bl} - T_{cl}) \exp\left(\frac{r - r_l}{r r_l a_l}\right), \tag{82}$$

with the constants

$$T_{cl} = \frac{Q_i}{j_i c_l} + T_0, \quad a_l = \frac{\kappa_l}{j_i r_i^2 c_l}. \tag{83}$$

Note that by Eqs. (81) and (83), the constants T_{cl} and T_{cv} depend on the values of the interface fluxes, j_i and Q_i, which in turn are functions of the temperatures T_l and T_v directly at the interface, as computed in Secs. IV and V,

$$j_i = \mathcal{J}(T_l, T_v), \quad Q_i = \mathcal{Q}(T_l, T_v). \tag{84}$$

As in the planar case, Eqs. (80)–(84) form a nonlinear set of equations for the four constants T_l, T_v, j_i, and Q_i, which must be solved numerically.

Here it must be mentioned that we derived the interface mass and energy fluxes (40) for the special case of planar geometry. The results can be used for spherical interfaces as long as surface tension effects play no role. When surface tension effects are important, the saturation pressure must be corrected according to (see, e.g., Ref. [10])

$$p'_{sat}(T) = p_{sat}(T) \exp\left(\frac{2\eta}{r_c} \frac{v}{RT}\right), \tag{85}$$

where η is the surface tension coefficient and r_c is the radius of curvature. We estimate the correction for the case of water at $T = 273$ K, which has a surface tension coefficient of $\eta = 7.27 \times 10^{-2}$ J/m^2 [46], and a specific volume of $v = 10^{-3}$ m^3/kg. The correction factor becomes $\exp(1.15 \times 10^{-9}\ \text{m}/r_c)$, and this gives a correction above 1%, if the radius of curvature is less than 1.15×10^{-9} m/ln $1.01 = 1.16 \times 10^{-7}$ m. For larger radii, as encountered in the Toronto experiments, surface tension effects can be neglected.

VIII. SOME SIMPLE ESTIMATES

A. Planar case

In order to understand the relation between experiment and equations better, we discuss the experiments and equations together based on simple estimates of the magnitude of various terms. In order to have an easier access, we consider the case where $\omega = 0$; i.e., the condensation coefficient is independent of the impact energy. In this case the mass flow through the interface is given by Eq. (42) which can be manipulated to give

$$p_{sat}(T_l) \sqrt{\frac{T_v}{T_l}} - p_v = \frac{2 - \psi}{\psi} \sqrt{\frac{\pi}{2} R T_v} j. \tag{86}$$

The measured value of the mass flow is about $j = 1. \times 10^{-3}$ kg/(m^2 s), and for a vapor temperature of 280 K we obtain $\sqrt{(\pi/2) R T_v} j \simeq 0.45$ Pa which is three orders of mag-

nitude smaller than the pressure $p_v \simeq 600$ Pa. It follows that the difference between p_v and $p_{sat}(T_l)\sqrt{T_v/T_l}$ is very small, as long as the condensation coefficient ψ is not too small. Since the measurements indicate that the temperature difference between vapor and liquid is not more than 1% or 2%, it follows that $p_{sat}(T_l) \simeq p_v$ which implies that the liquid temperature at the interface is close to the saturation temperature at the prescribed vapor pressure $T_l \simeq T_{sat}(p_v)$. Only when the condensation coefficient is small—e.g., $\psi < 0.05$—will a marked difference between the two pressures be observed.

We proceed to discuss the case for sufficiently large condensation coefficient, where $T_l \simeq T_{sat}(p_v)$, by turning our attention to the energy balance (59). Note that the exponentials in Eqs. (70) and (71) can be reduced to linear functions for small mass flows, where the coefficients a_l and a_v become small. Then we can replace the differentials by finite differences, and the equation can be rewritten as

$$j(h_v - h_l) = \frac{\kappa_v}{L_v}(T_{bv} - T_v) - \frac{\kappa_l}{L_l}(T_l - T_{bl}).$$

While the difference $h_v - h_l$ depends on the local temperatures of liquid and vapor, it is mainly determined by the enthalpy of evaporation, so that we can set $h_v - h_l \simeq \Delta h_0$. Moreover, in good agreement with the experiment, we set $T_{bv} - T_v \simeq T_{bl} - T_l$, which implies that the temperature jump at the interface is ignored for this argument, and equal boundary temperatures are assumed. With all assumptions used, we obtain

$$j \simeq \left[\frac{\kappa_v}{L_v} + \frac{\kappa_l}{L_l}\right]\frac{T_{bl} - T_{sat}(p_v)}{\Delta h_0} \simeq \frac{\kappa_l}{L_l}\frac{T_{bl} - T_{sat}(p_v)}{\Delta h_0}. \quad (87)$$

With the data from the experiment in Table I, this rough estimate yields

$$j \simeq 1.2 \times 10^{-3}\ \mathrm{kg/(m^2\,s)},$$

which is surprisingly close to the measured value. Note that the contribution of the vapor heat conductivity can be ignored here, since $\kappa_v/L_v \ll \kappa_l/L_l$.

We emphasize that this estimate is independent of the value for the evaporation coefficient. Our numerical simulations agree well with this value and with the statement that the condensation coefficient has only little influence on the evaporation mass flow. The very weak dependence of the evaporation mass flow on the condensation coefficient might give an explanation of why measured values of the condensation coefficient assume a wide variety of values.

A similar estimate can be performed on the phenomenological laws (50) and (52), which would lead to the same conclusion—namely, that the liquid interface temperature is close to the saturation temperature $T_{sat}(p_v)$ and that the evaporation mass flux is approximately given by Eq. (87). In this case, the evaporation mass flow is not much influenced by the phenomenological coefficient β which here plays a similar role as the condensation coefficient does in the kinetic theory based models. Again, this agrees with our numerical simulations.

B. Spherical geometry

We consider the same problem for the spherical case, which seems to better match the geometry of the experiment, in particular for the funnel. We start by introducing the interface temperatures into the expressions for temperature, Eqs. (80) and (82), which yields, for the gradients,

$$\frac{dT_v(r)}{dr} = \frac{T_{bv} - T_v}{a_v r^2}\frac{\exp\left(\dfrac{r - r_v}{r r_v a_v}\right)}{1 - \exp\left(\dfrac{r_i - r_v}{r_i r_v a_v}\right)},$$

$$\frac{dT_l(r)}{dr} = \frac{T_{bl} - T_l}{a_l r^2}\frac{\exp\left(\dfrac{r - r_l}{r r_l a_l}\right)}{1 - \exp\left(\dfrac{r_i - r_l}{r_i r_l a_l}\right)}.$$

The energy balance directly at the interface can be written as

$$j_i h_{v|i} - \kappa_v \left.\frac{dT_v(r)}{dr}\right|_i = j_i h_{l|i} - \kappa_l \left.\frac{dT_l(r)}{dr}\right|_i$$

or with the above expressions, for the gradients,

$$j_i h_{v|i} - \frac{T_{bv} - T_v}{\dfrac{a_v}{\kappa_v} r_i^2}\frac{1}{\exp\left(-\dfrac{r_i - r_v}{r r_v a_v}\right) - 1} = j_i h_{l|i} - \frac{T_{bl} - T_l}{\dfrac{a_l}{\kappa_l} r_i^2}\frac{1}{\exp\left(-\dfrac{r_i - r_l}{r_i r_l a_l}\right) - 1}.$$

As above, we assume that $T_{bl} - T_l \simeq T_{bv} - T_v$ and $T_l = T_{sat}(p_v)$, so that

$$j_i(h_{v|i} - h_{l|i}) = [T_{bl} - T_{sat}(p_v)]\left[\frac{\kappa_v}{a_v r_i^2}\frac{1}{\exp\left(-\dfrac{r_i - r_v}{r_i r_v a_v}\right) - 1} - \frac{\kappa_l}{a_l r^2}\frac{1}{\exp\left(-\dfrac{r_i - r_l}{r_i r_l a_l}\right) - 1}\right].$$

Next we use the definitions of the coefficients a_l and a_v in Eqs. (81) and (83) and assume, again, that we can expand the exponentials since their arguments are reasonably small, to obtain

$$j_i = \frac{\kappa_l}{L_l}\frac{T_{bl} - T_{sat}(p_v)}{\Delta h_0}\Lambda, \quad (88)$$

where

$$\Lambda = \frac{L_l}{r_l}\left[\frac{\dfrac{\kappa_v r_l}{\kappa_l r_i} + \dfrac{\dfrac{r_l}{r_i}}{\dfrac{r_i}{r_l} + 1}}{1 - \dfrac{r_i}{r_v}}\right].$$

This expression differs from the estimate for the planar case (87) by the factor Λ, which we obtain as $\Lambda = 0.193$ by choos-

ing the following values, suggested by the experiment: $r_i = 6$ mm, $r_v = r_i + L_v = 24.5$ mm, and $r_l = r_i - L_l = 1$ mm. In other words, geometric effects give an approximately 5 times smaller evaporation flow than in the planar case.

C. Heat flux and interface temperature jump

The above arguments did not use the expression for the energy flux Q at the interface, which, however, comes into play to determine the temperature jump $T_v - T_l$ at the interface. We shall not try to estimate this temperature difference, but refer the reader to our numerical solutions presented below. Nevertheless, we give a qualitative discussion. First we recall from the discussion above that the evaporation mass flux is largely independent of the condensation coefficients (or phenomenological coefficients). We can rewrite Eqs. (59) and (76) as

$$\mathcal{Q}(T_l, T_v) - \mathcal{J}(T_l, T_v) h_v(T_v) = -\kappa_v \left(\frac{dT}{dz}\right)\bigg|_{v,i}. \tag{89}$$

which relates the temperature T_l to the temperature T_v and its gradient at the interface $(dT/dr)|_{v,i}$ in an implicit manner. Note that the liquid interface temperature T_l follows from Eq. (86), so that Eq. (89) serves to compute T_v.

In case of spherical symmetry, one will find the gradient $(dT/dr)|_{v,i}$ instead, but the argument will be the same, and the left-hand side of the equation will remain unchanged as well. To estimate the gradients, we use the same approximations as in the above subsections to find

$$\left(\frac{dT}{dz}\right)\bigg|_{v,i} \simeq \frac{T_{bv} - T_v}{L_v}, \quad \left(\frac{dT}{dr}\right)\bigg|_{v,i} \simeq \frac{T_{bv} - T_v}{L_v}\left(1 + \frac{L_v}{r_i}\right), \tag{90}$$

where we have also used $r_v = r_i + L_v$. With the experimental data used at the end of the last section ($r_i = 6$ mm, $L_v = 18.5$ mm) follows that the gradient of the vapor temperature in spherical geometry is about 4 times larger then the gradient in planar geometry. This is a remarkable change which has marked influence on the size of the temperature jump, as will be shown below.

For the TIP model, Eq. (89) reduces to

$$\alpha\left(\frac{1}{T_v} - \frac{1}{T_l}\right) = -\kappa_v \frac{T_{bv} - T_v}{L_v}\Gamma,$$

where $\Gamma = 1$ in planar geometry and $\Gamma = 1 + L_v/r_i$ in spherical geometry. This can be written as

$$\left(1 + \frac{\alpha L_v}{\Gamma \kappa_v}\frac{1}{T_l T_v}\right)(T_v - T_l) = T_{bv} - T_l.$$

This shows that $T_v > T_l$ as long as $T_{bv} - T_l > 0$; both conditions are observed in the experiment. Note that the temperature jump in TIP, as estimated above, is determined only by the phenomenological law for Q (or q_v) at the interface and is independent of the evaporation rate j.

The obvious conclusion of this section is that (a) a large temperature gradient of the vapor at the interface yields a larger temperature jump and that (b) spherical geometry gives a larger gradient and, therefore, favors larger jumps.

TABLE II. Evaporation experimental data of Ward *et al.*

Experiment	p_v (Pa)	T_{bl} (°C)	L_l (mm)	T_{bv} (°C)	L_v (mm)	r_i (mm)	L_c (mm)
$E1$	593	26.06	4.97	25.7	18.59	6.088	0.34

D. Heat leaks and geometry

The above arguments show that the temperature of the liquid is close to the saturation temperature T_{sat} at the prescribed pressure in the vapor p_v and the evaporation rate depends predominantly on the heat transferred through the liquid to the interface, where liquid evaporates.

The amount of heat flowing into the interface depends on the temperature of the liquid at the interface, the geometry of the experimental apparatus, and the temperatures at the boundaries of the apparatus. Accordingly, one can expect a good match between theory and experiment only if the simulation of the experiment includes an accurate setup of the experiment. While this is outside the scope of the present paper, we continue to discuss the Toronto experiments on the base of this observation.

Since in the Toronto experiments the evaporation rate is slow and the liquid enthalpy small, this heat is provided through nonconvective heat transfer. Therefore we can say that the evaporation rate is limited through the conductive heat transfer in the liquid. The measured evaporation rate is $j_{\text{experiment}} \simeq 1.017 \times 10^{-3}$ kg/(m^2 s) and the value predicted for the planar case, $j_{\text{planar}} \simeq 1.2 \times 10^{-3}$ kg/(m^2 s), is relatively close to the measured value. However, the value predicted for the actual—spherical—funnel geometry, $j_{\text{spherical}} = 2.34 \times 10^{-4}$ kg/(m^2 s), is far too low. The dominant factor which gives the reduced evaporation rate in the spherical case is the second term in Λ, Eq. (88), which is due to the heat transfer in the liquid.

The above argument assumes that the funnel walls are adiabatic, so that all heat is drawn from the funnel inlet, where the temperature is maintained at T_{bl}. As this heat flows through the liquid in the funnel, it is distributed over the larger and larger cross sections of the funnel, and thus less heat can be provided per unit area of the interface.

Since the observed evaporation flux is larger than predicted, we must conclude that the funnel walls are not adiabatic, so that a substantial amount of heat (enough to give an approximately 5 times larger evaporation rate) creeps in through the funnel walls.

In this context we recall that Ward and Stanga suggest that the temperature gradient in the liquid is constant [4], which would be expected in the planar case. Note, however, that the liquid temperature measurements are concentrated near the interface, with only one measurement at the liquid boundary. Additional measurement points in the liquid region would be necessary to understand the transport in the liquid better and to confirm the constant liquid temperature gradient.

In an effort to model the experiment in a simple, but sufficiently accurate manner, we also model the liquid according

TABLE III. Geometry dependent simulation results, SRT.

Model	T_l (°C)	T_v (°C)	j [kg/(m^2 s)]
Measured	−0.4	2.6	1.017×10^{-3}
SRT planar-planar	−0.33	0.0098	1.27×10^{-3}
SRT planar-spherical	−0.33	2.67	1.29×10^{-3}
SRT spherical-spherical	−0.34	3.26	2.47×10^{-4}

to the planar case and the vapor according to the equations for the spherical case. To combine a planar description of the liquid with a spherical description of the liquid, it is necessary to choose a common coordinate system. We chose a frame where the interface is at $z=0$, so that have at the interface, $z=0$ and $r=r_i$. This implies $z=r-r_i$, $r_v=r_i+L_v$, and $r_l=r_i-L_l$.

E. Constant temperature zone in liquid

Ward and Stanga [4] observe a small isothermal zone of thickness L_c in the liquid adjacent to the interface, which they suggest could be due to surface tension driven Marangoni-Benard convection or energy partitioning during the phase change process. Our simplified models do not allow for either of these phenomena and thus do not predict a liquid isothermal zone. In order to be able to compare with the experiments, we artificially introduced a small isothermal zone into the simulations. The only effect of this is that the effective liquid thickness becomes a bit smaller—i.e., $L_{l\mid\mathrm{eff}}=L_l-L_c$.

IX. MODELING RESULTS

A. Models used and setup

With the aforementioned considerations, we present the evaporation results using the constant liquid temperature zone and purely planar, purely spherical, and mixed planar and spherical geometries. These geometries differ considerably from the geometry of the experiments, and therefore the reader will not expect perfect agreement between simulations and experimental data. However, this study allows the understanding of the basic trends and, in particular, the strong importance of geometry on the outcome.

The results depend on the choice of models for the interface expressions for mass and energy flow, and we shall use the following models for simulations.

CE: A classical kinetic theory model, based on the Chapman-Enskog expansion with condensation coefficient $\theta_c=\psi=1$, Eqs. (41), the standard Schrage model [1].

CEVEL: A kinetic theory model, based on the Chapman-Enskog expansion and the velocity dependent condensation coefficient (15), with variable accommodation coefficient, Eqs. (40).

SRT: A phenomenological model, comprised of the SRT mass flow (52) and (53) and the phenomenological law (51) for the heat flux.

The CE model includes no free parameters, while the CEVEL model can be fitted to experimental data by adjusting the parameters ψ, ω, and γ. Other models based on kinetic theory are not considered here, but were tested as well. The results showed in particular that there was no marked difference between the models based on the Chapman-Enskog distribution and those based on the Maxwellian, Eqs. (26) and (28). Since this refers only to the particular setting of the Toronto experiments, we do not wish to draw further conclusions from this result.

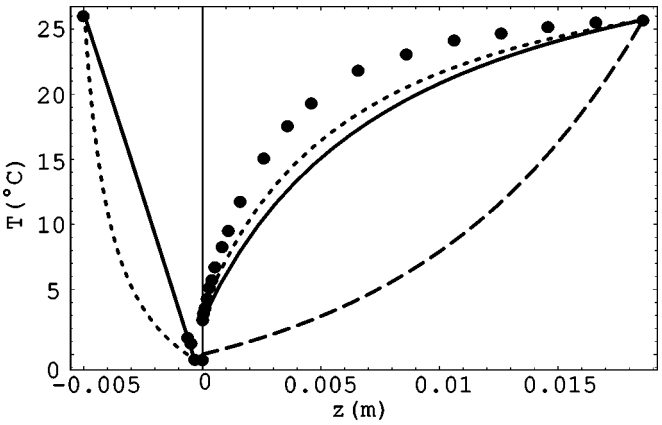

FIG. 5. Temperature profiles for SRT simulations with $\alpha=1.37\times10^6$ (W K)/m^2. Planar-planar geometry (dashed line), planar-spherical geometry (solid line), spherical-spherical geometry (dotted line), and experimental results (dots).

The SRT model has only one adjustable parameter, which is the phenomenological coefficient α. For the data in the experiment the nonlinear expression (52) yields the same results as the linear expression (54), which agrees with the general phenomenological law (50). Moreover, as our estimates in Sec. VII showed, the parameter β in the phenomenological models has no marked influence on the results, and this finding was supported by numerical tests. For space reasons, we present only solutions which use $\beta=\beta_{SRT}$ as given in Eq. (55).

Table II shows the controlled data for one of the experiments performed by Ward and Stanga [4,47]; other experiments were similar. We chose the parameters in the models—i.e., the coefficients ψ, ω, γ, and α—where applicable so that the simulations stand in reasonable agreement with the measurements.

B. SRT simulations

In this case, we only need to specify the phenomenological coefficient for heat transfer, which we chose as $\alpha=1.37\times10^6$ (W K)/m^2. Table III shows the interface temperatures and the mass flow j for the different geometries in comparison to the experiment. As expected and discussed above, the planar geometry for the liquid gives a reasonable mass flow not to far from the experimental value, while in spherical geometry of the liquid the heat flow to the interface is limited, which results in a low evaporation rate. The geometry has a strong influence on the temperature difference between vapor and liquid at the interface, which is much larger in case of spherical geometry for the vapor than in the planar case.

TABLE IV. Geometry dependent simulation results, CE.

Model	T_l (°C)	T_v (°C)	j [kg/(m^2 s)]
Measured	−0.4	2.6	1.017×10^{-3}
CE planar-planar	−0.33	−0.39	1.27×10^{-3}
CE planar-spherical	−0.33	−0.35	1.30×10^{-3}
CE spherical-spherical	−0.34	−0.29	2.51×10^{-4}

Figure 5 shows the temperature profiles for the three cases. Of particular importance is the large temperature gradient in the vapor at the interface for the spherical cases, which leads to the larger temperature jump. Note that the curvature of the temperature profiles agrees with the experiment in the spherical case, whereas the planar case gives opposite curvature. Finally we note that in all cases the liquid temperature is very close to the saturation temperature $T_{sat}(p_v)$, as measured.

Altogether we can state that the SRT model (52) and (53) with the TIP expression for the interface energy flux, Eq. (51), gives a good description of the Toronto evaporation experiments.

C. CE model

The classical Schrage model [1], Eqs. (41), has no adjustable coefficients, and Table IV gives the results for interface temperature and mass flow. The liquid temperature is again equal to the saturation temperature $T_{sat}(p_v)$, and the mass flux j has almost the same values as in the SRT case. This is expected since we have shown that the evaporation rate depends mostly on the heat transferred through the liquid, which is independent of the model for j at the interface. The vapor temperature at the liquid is very close to the liquid temperature and slightly lower in the planar cases, while the vapor has a higher temperature in the purely spherical case. In all cases the temperature jump is small and far from that obtained in the experiments.

Altogether it follows that the classical Schrage model cannot describe the experiment with sufficient accuracy, since it does not give an interface temperature jump of sufficient magnitude.

D. CEVEL model

With models based on the velocity dependent condensation coefficient we can vary the parameters ψ, ω, and γ to obtain agreement with the experiments. We first show results for a case with relatively low condensation coefficient, strong velocity dependence, and purely specular reflection of noncondensing particles, where $\psi=0.05$ and $\omega=\gamma=1$. Interface temperatures and mass flow are given in Table V. Figure 6 shows the corresponding temperature curves.

Again, the evaporation rate is very close to the SRT case, for the same reasons as discussed for the CE model. Due to the relatively small condensation coefficient, the liquid temperature is now about 1 °C above the saturation temperature $T_{sat}(p_v)$, in agreement with our discussion of Eq. (86).

TABLE V. Geometry dependent simulation results, CEVEL, with $\psi=0.05$, $\omega=\gamma=1$.

Model	T_l (°C)	T_v (°C)	j [kg/(m^2 s)]
Measured	−0.4	2.6	1.017×10^{-3}
CEVEL planar and planar	0.6172	0.6165	1.22×10^{-3}
CEVEL planar and spherical	0.63	3.12	1.25×10^{-3}
CEVEL spherical and spherical	−0.15	3.41	2.45×10^{-4}

The temperature jump at the interface is positive for spherical vapor geometry and is as large as measured. Note that a small negative temperature jump is predicted in purely planar geometry.

In order to better understand the influence of the coefficients, we study the case $\psi=0.1$ and $\omega=\gamma=1$; that is, we assume that a larger portion of vapor particles will condense. The results in Table VI indicate that this leads to a lower liquid temperature, which is now closer to the saturation temperature $T_{sat}(p_v)$, and to a smaller temperature jump. The evaporation rate is almost not affected.

Next we study the influence of the accommodation coefficient, by considering $\psi=0.05$, $\omega=1$, and $\gamma=0$; see Table VII. We see that this change leaves the liquid temperature unaffected in comparison to the first case, Table V but reduces the temperature jump. Thus we can conclude that an accommodation coefficient close to unity will favor a larger temperature jump. This makes sense, since a small accommodation coefficient implies many thermalizing collisions between vapor and liquid and, hence, a better exchange of energy that supports equilibration of temperatures.

Next we consider a case where all vapor particles condense, $\psi=1$ and $\omega=1$ (note that γ plays no role in this case) (Table VIII). Now the liquid temperature is equal to the saturation temperature $T_{sat}(p_v)$, but the temperature jump is negative (and small) for planar liquid geometry and positive but very small for the purely spherical case. The results are close to those of the CE model (Table IV).

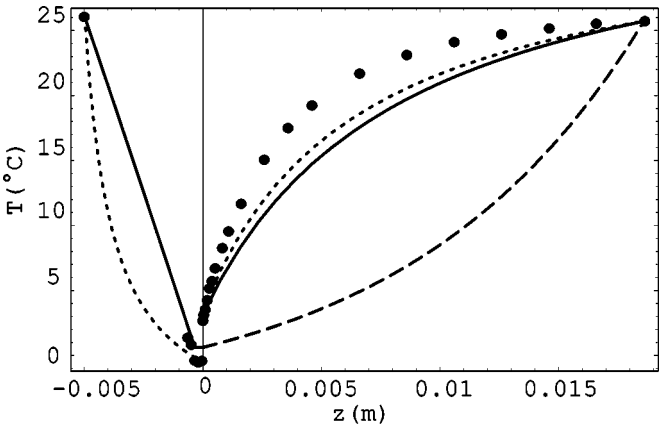

FIG. 6. Temperature profiles for CEVEL simulations with $\psi=0.05$ and $\omega=\gamma=1$. Planar-planar geometry (dashed line), planar-spherical geometry (solid line), spherical-spherical geometry (dotted line), and experimental results (dots).

TABLE VI. Geometry dependent simulation results, CEVEL, with $\psi=0.1$, $\omega=\gamma=1$.

Model	T_l (°C)	T_v (°C)	j [kg/(m^2 s)]
Measured	−0.4	2.6	1.017×10^{-3}
CEVEL planar-planar	0.14	−0.038	1.25×10^{-3}
CEVEL planar-spherical	0.15	1.34	1.27×10^{-3}
CEVEL spherical-spherical	−0.24	1.62	2.48×10^{-4}

TABLE VIII. Geometry dependent simulation results, $\psi=\omega=1$.

Model	T_l (°C)	T_v (°C)	j [kg/(m^2 s)]
Measured	−0.4	2.6	1.017×10^{-3}
CEVEL planar-planar	−0.31	−-0.667	1.27×10^{-3}
CEVEL planar-spherical	−0.31	−0.57	1.30×10^{-3}
CEVEL spherical-spherical	−0.33	−0.27	2.51×10^{-4}

Finally, we ask for the influence of the coefficient ω, which determines the importance of the impact energy on the condensation probability. For this, we consider $\psi=0.1$, $\omega=0.5$, and $\gamma=1$. From the results in Table IX follows that a smaller value of ω leads not only to a smaller temperature jump, but also to a different sign: for planar liquid geometry the temperature jump is negative, while it becomes positive in the purely spherical case.

Summarizing we can conclude that a kinetic theory model with velocity dependent condensation coefficient can give large and positive temperature jumps between vapor and liquid at the interface. However, large temperature jumps require that only a small portion of vapor molecules that hit the interface condense (small values of ψ), that those particles that do not condense do not exchange much energy with the liquid (γ close to unity), and that the condensation probability for fast particles be much higher than that for slow particles (ω close to unity).

Moreover, the comparison of different geometries shows that size and sign of the temperature jump depend strongly on the geometry.

In particular we note that for the model presented here a large temperature jump is accompanied by a liquid interface temperature above the saturation temperature $T_{sat}(p_v)$ which does not agree well with experiments, where the liquid interface is found at the saturation temperature.

X. CONCLUSIONS

In this paper, we used kinetic theory arguments to derive expressions for the mass and energy fluxes at liquid-vapor interfaces in nonequilibrium. In particular we based the calculations on a condensation coefficient that depends on the impact energy of the condensing particle normal to the interface, as suggested from molecular dynamics simulations. This leads to a generalization of the well-known Hertz-Knudsen and Schrage laws for the evaporation and condensation rates, which now depend on parameters that describe the velocity dependent particle condensation probability.

We also briefly reviewed basic expressions for the interface fluxes that were derived by the methods of thermodynamics of irreversible processes and statistical rate theory.

Then we considered these models for evaporation in simple geometries, in particular 1D planar and 1D spherical transport, in order to describe and understand the experiments recently performed in Toronto by Ward, Fang, and Stanga.

A particularly interesting feature in the experiments is the observation of a distinct temperature jump at the interface between vapor and liquid, where the vapor temperature is higher than the liquid temperature. Standard kinetic theory models predict only a very small negative temperature difference, where the liquid has a slightly higher temperature.

Our considerations revealed that the direction of the temperature jump depends on geometry, and we presented cases where even with the standard Schrage model (CE) the vapor temperature was higher. The inclusion of the velocity dependent condensation coefficient leads to more refined models (CEVEL), with several parameters that can be adjusted to give much larger interface temperature jumps, as observed in the experiments.

The coefficients in the phenomenological models can also be adjusted to yield the observed temperature jumps. Here we used only very simple models, which ignored the cross coupling of thermodynamic fluxes and forces. While these simple models were sufficient to reproduce the general trends, it is likely that cross effects must be considered to achieve a perfect modeling of the experiments. However, this will require an exact simulation of the experiment, including its geometry, and therefore this question was not further considered in the present work.

A simple analysis, which is supported by our numerical results, showed that, at least for the conditions in the Toronto experiments, the evaporation and condensation mass flux is mostly driven by energy flow, while the equation for the

TABLE VII. Geometry dependent simulation results, CEVEL, with $\psi=0.05$, $\omega=1$, $\gamma=0$.

Model	T_l (°C)	T_v (°C)	j [kg/(m^2 s)]
Measured	−0.4	2.6	1.017×10^{-3}
CEVEL planar-planar	0.6172	0.6852	1.23×10^{-3}
CEVEL planar-spherical	0.63	0.75	1.25×10^{-3}
CEVEL spherical-spherical	−0.14	−0.068	2.45×10^{-4}

TABLE IX. Geometry dependent simulation results, $\psi=0.1$, $\omega=0.5$, $\gamma=1$.

Model	T_l (°C)	T_v (°C)	j [kg/(m^2 s)]
Measured	−0.4	2.6	1.017×10^{-3}
CEVEL planar-planar	0.0022	−1.19	1.26×10^{-3}
CEVEL planar-spherical	−0.0082	−0.195	1.28×10^{-3}
CEVEL spherical-spherical	−0.296	0.83	2.49×10^{-4}

mass flow essentially determines the liquid interface temperature (Sec. IX). The latter is almost independent of the coefficients that appear in the interface mass flow expression, which implies that these can have almost arbitrary values and still give results in very good agreement with experimental data. This is the most likely reason why a wide variety of values for these coefficients can be found in the literature.

The interface temperature jump depends on the expression for the interface energy flux, and the choice of parameters in these is crucial for a good agreement with the experiments. This is of particular importance for the SRT model: SRT gives an interesting and well-founded expression for the interface mass flux, but does not provide an expression for the interface energy flow. It would be very interesting to use SRT arguments to find such an expression.

We do not claim that our simulations of the experiments are perfect. The two most important shortcomings are that we modeled the water vapor as a monatomic ideal gas and that we used very simplified geometries.

To model water vapor more realistically, the kinetic theory treatment must be extended to incorporate the internal degrees of freedom of the molecules. This was beyond the scope of this paper, which aimed at first showing that velocity dependent condensation coefficients allow to better model experiments than constant condensation coefficients.

Our discussion shows that details of the geometries of the experimental apparatus and heat leaks have significant influence on the experimental findings. A thorough understanding of experiments—e.g., the Toronto evaporation and condensation experiments—can only be achieved by accurately modeling the experiments in all detail.

ACKNOWLEDGMENT

This research was supported by the Natural Sciences and Engineering Research Council (NSERC).

[1] R. W. Schrage, *A Theoretical Study of Interphase Mass Transfer* (Columbia University Press, New York, 1953).
[2] G. Fang and C. A. Ward, Phys. Rev. E **59**, 417 (1999).
[3] G. Fang and C. A. Ward, Phys. Rev. E **59**, 441 (1999).
[4] C. A. Ward and D. Stanga, Phys. Rev. E **64**, 051509 (2001).
[5] H. Hertz, Ann. Phys. (Leipzig) **17**, 177 (1882).
[6] M. Knudsen, Ann. Phys. (Leipzig) **47**, 697 (1915).
[7] Y. P. Pao, Phys. Fluids **14**, 306 (1971).
[8] Y. P. Pao, Phys. Fluids **14**, 1340 (1971).
[9] Y. Sone and Y. Onishi, J. Phys. Soc. Jpn. **44**, 1981 (1978).
[10] J. B. Young, Int. J. Heat Mass Transfer **34**, 1649 (1991).
[11] Y. Sone, *Kinetic Theory and Fluid Dynamics* (Birkhauser, Boston, 2000).
[12] R. Meland, A. Frezzotti, T. Ytrehus, and B. Hafskjold, Phys. Fluids **16**, 223 (2004).
[13] K. Yasuoka and M. Matsumoto, J. Chem. Phys. **101**, 7904 (1994).
[14] M. Matsumoto, Fluid Phase Equilib. **144**, 307 (1998).
[15] R. Meland and T. Ytrehus, in *Rarefied Gas Dynamics: 22nd International Symposium*, edited by T. J. Bartel and M. A. Gallis, AIP Conf. Proc. No. 585 (AIP, Melville, NY, 2001), p. 583.
[16] T. Tsuruta, H. Tanaka, and T. Masuoka, Int. J. Heat Mass Transfer **42**, 4107 (1999).
[17] G. Nagayama and T. Tsuruta, J. Chem. Phys. **118**, 1392 (2003).
[18] T. Tsuruta and G. Nagayama, Therm. Sci. Eng. **10**, 9 (2002).
[19] S. R. de Groot and P. Mazur, *Non-equilibrium Thermodynamics* (Dover, New York, 1984).
[20] D. Bedeaux, Adv. Chem. Phys. **64**, 47 (1986).
[21] D. Bedeaux, L. J. F. Hermans, and T. Ytrehus, Physica A **169**, 263 (1990).
[22] D. Bedeaux and S. Kjelstrup, Physica A **270**, 413 (1999).
[23] C. A. Ward and G. Fang, Phys. Rev. E **59**, 429 (1999).
[24] C. A. Ward, J. Non-Equilib. Thermodyn. **27**, 289 (2002).
[25] L. Koffman, M. Plesset, and L. Lees, Phys. Fluids **27**, 876 (1984).
[26] R. Meland and T. Ytrehus, Phys. Fluids **16**, 836 (2004).
[27] S. Kjelstrup, T. Tsuruta, and D. Bedeaux, J. Colloid Interface Sci. **256**, 451 (2002).
[28] P. N. Shankar and M. Deshpande, Phys. Fluids A **2**, 1030 (1990).
[29] D. Bedeaux, E. Johannessen, and A. Rosjorde, Physica A **330**, 329 (2003).
[30] E. Johannessen and D. Bedeaux, Physica A **330**, 354 (2003).
[31] E. Johannessen and D. Bedeaux, Physica A **336**, 252 (2004).
[32] C. Cercignani, *Rarefied Gas Dynamics From Basic Concepts to Actual Calculations* (Cambridge University Press, Cambridge, England, 2000).
[33] S. Harris, *An Introduction to the Theory of the Boltzmann Equation* (Holt, Rinehart, and Winston, New York, 1971).
[34] G. A. Bird, *Molecular Gas Dynamics and the Simulation of Gas Flows* (Clarendon Press, Oxford, 1994).
[35] S. Chapman and T. Cowling, *The Mathematical Theory of Non-uniform Gases*, (Cambridge University Press, Cambridge, England, 1970).
[36] A. K. Rebrov, in *Rarefied Gas Dynamics: 22nd International Synposium*, edited by T. J. Bartel and M. A. Gallis, AIP Conf. Proc. No. 585 (AIP, Melville, NY, 2001), p. 557.
[37] R. Meland and T. Ytrehus, Phys. Fluids **15**, 1348 (2003).
[38] I. Eames, N. Marr, and H. Sabir, Int. J. Heat Mass Transfer **40**, 2963 (1997).
[39] R. Marek and J. Straub, Int. J. Heat Mass Transfer **44**, 39 (2001).
[40] J. Barrett and C. Clement, J. Colloid Interface Sci. **150**, 352 (1992).
[41] T. Ytrehus, Rarefied Gas Dyn. **51**, 1197 (1977).
[42] B. Bird, W. E. Stewart, and E. N. Lightfoot, *Transport Phenomena* (Wiley, New York, 1960).
[43] *Handbook of Chemistry and Physics*, 59th ed., edited by W. Robert and M. J. Astle (CRC Press, West Palm Beach, FL, 1978).

[44] M. W. Bond, M.A.Sc. thesis, University of Victoria, BC, Canada, 2004.

[45] S. Wolfram, *The Mathematica Book*, 4th ed. (Wolfram Media/ Cambridge University Press, Cambrigde, England, 1999).

[46] M. Kaufman, *Principles of Thermodynamics* (Marcel Dekker, New York, 2002).

[47] C. A. Ward, Temperature Profile Data Points, 2001, email communication, 2003.